

Western  Graduate&PostdoctoralStudies

Western University  
**Scholarship@Western**

---

Electronic Thesis and Dissertation Repository

---

8-2-2016 12:00 AM


# Unravelling The Subfields Of The Hippocampal Head Using 7-Tesla Structural MRI

Jordan M. K. DeKraker  
*The University of Western Ontario*

Supervisor  
Dr. Stefan Köhler  
*The University of Western Ontario*

Graduate Program in Psychology  
A thesis submitted in partial fulfillment of the requirements for the degree in Master of Science  
© Jordan M. K. DeKraker 2016

Follow this and additional works at: <https://ir.lib.uwo.ca/etd>

 Part of the [Cognitive Neuroscience Commons](#), [Computational Neuroscience Commons](#), [Nervous System Commons](#), [Other Neuroscience and Neurobiology Commons](#), and the [Tissues Commons](#)

---

## Recommended Citation

DeKraker, Jordan M. K., "Unravelling The Subfields Of The Hippocampal Head Using 7-Tesla Structural MRI" (2016). *Electronic Thesis and Dissertation Repository*. 3918.  
<https://ir.lib.uwo.ca/etd/3918>

This Dissertation/Thesis is brought to you for free and open access by Scholarship@Western. It has been accepted for inclusion in Electronic Thesis and Dissertation Repository by an authorized administrator of Scholarship@Western. For more information, please contact [wlsadmin@uwo.ca](mailto:wlsadmin@uwo.ca).

## Abstract

Probing the functions of human hippocampal subfields is a promising area of research in cognitive neuroscience. However, defining subfield borders in Magnetic Resonance Imaging (MRI) is challenging. Here, we present a user-guided, semi-automated protocol for segmenting hippocampal subfields on T2-weighted images obtained with 7-Tesla MRI. The protocol takes advantage of extant knowledge about regularities in hippocampal morphology and ontogeny that have not been systematically considered in prior related work. An image feature known as the hippocampal ‘dark band’ facilitates tracking of subfield continuities, allowing for unfolding and segmentation of convoluted hippocampal tissue. Initial results suggest that this protocol offers sufficient precision and flexibility to accommodate inter-individual differences in morphology and produces segmentations that have improved accuracy and detail compared to other prominent protocols, with similar inter-rater reliability. We anticipate that this protocol will allow for improved anatomical precision in future research on hippocampal subfields in health and neurological disease.

## Keywords

Hippocampus, Hippocampal subfields, Uncus, Cytoarchitecture, Magnetic Resonance Imaging, 7-Tesla, Morphometry, Tissue Segmentation, Laplacian equation, Fast Marching algorithm

## Co-Authorship Statement

Dr. Köhler oversaw the project, and coordinated the efforts of the other contributors. He contributed significantly to the background research and motivation for the current project, in particular focusing on the need for better anatomical specificity and MRI research and the idea that ontogeny could provide unique cues to guide subfield segmentation.

Dr. Khan helped in overseeing the project, and contributed significantly to the research into and application of 3D computational image processing techniques. He guided high-level discussions on these tools and their application, and directly applied some of them. He helped troubleshoot and suggested new techniques and software packages that could contribute to the project. He also collected and preprocessed the MRI data.

Kayla Ferko performed much of the manual segmentation presented in this study, and contributed to discussions about available MRI features and challenges for reliably segmenting the hippocampus from surrounding structures.

## Acknowledgments

Thanks to everybody in the Köhler lab for constructive discussions and encouragements. Thanks to Dr. Köhler for his constant guidance and insightful feedback at all stages of this project. Thanks to Dr. Khan for teaching me many of the skills required to carry out this project, and for his enthusiasm to pursue new directions.

Thanks to my girlfriend, Samantha Chin, for her support, and my friends inside and outside of academia for always being willing to engage me in discussions about research. Thanks to my dad for suggested edits to my thesis, and to my mom for her wonderful and encouraging curiosity about science.

Thanks to the staff, faculty, and students at the Brain and Mind Institute for making it such a friendly and interesting place to work.

## Table of Contents

Abstract .....	ii
Co-Authorship Statement.....	iii
Acknowledgments.....	iv
Table of Contents .....	v
List of Tables .....	vii
List of Figures .....	viii
1. Introduction .....	1
1.1 Historical context of hippocampal research .....	1
1.2 Hippocampal subfield anatomy .....	3
1.3 Subfield-specific computational accounts of hippocampal function.....	5
1.4 Techniques for imaging the human hippocampal subfields .....	6
1.5 Techniques for segmenting hippocampal subfields in MR images .....	8
1.6 Challenges and limitations in current subfield tracing protocols .....	9
1.7 Recent advances in knowledge of subfield anatomy .....	11
1.8 Structural and developmental regularities .....	12
1.9 Goal of the current study .....	14
2 Methods.....	16
2.1 Participants .....	16
2.2 Image acquisition.....	16
2.3 Preprocessing.....	16
2.4 Generation of reference hippocampal models .....	17
2.5 Overview of segmentation protocol.....	18
2.6 Hippocampal grey matter .....	19

2.7	Computational techniques for dealing with convoluted tissues .....	21
2.8	Unfolding of hippocampal grey matter along anterior-posterior axis .....	22
2.9	Unfolding of hippocampal grey matter along proximal-distal axis.....	23
2.10	Defining subfield borders .....	24
2.11	Reliability measures.....	26
3	Results .....	28
3.1	Manually segmented reference hippocampi .....	28
3.2	Dark band dilation technique.....	30
3.3	Hippocampal grey matter unfolding .....	32
3.4	Completed segmentation morphologies .....	35
3.5	Reliability of manually traced and automatically segmented structures .....	37
3.6	Intensity differences across subfields .....	38
4	Discussion .....	41
4.1	Limitations elucidated by manually segmented reference hippocampi.....	41
4.2	Value and limitations of hippocampal grey matter unfolding .....	42
4.3	Consideration of completed subfield morphologies .....	44
4.4	Reliability of manually traced and automatically segmented structures .....	45
4.5	Future directions for further protocol improvement.....	47
4.6	Future applications.....	50
4.7	Conclusion .....	52
	References.....	53
	Appendix A: Manual and user-guided computational steps for hippocampal subfield labelling.....	58
	Appendix B: Mathematical definitions of computational unfolding techniques .....	70
	Curriculum Vitae .....	72

## List of Tables

Table 1. Mean volumes ( $\text{mm}^3$ ) of manually or user-guided segmented structures (dark band and hippocampal grey matter) and automatically segmented structures (subiculum - dentate gyrus) in left and right hippocampi. ....	36
Table 2. Inter- and intra-rater reliability measures (Dice Similarity Index) for manually or user-guided segmented structures (dark band and total hippocampal volume) and automatically segmented structures (subiculum - dentate gyrus). ....	38

## List of Figures

- Figure 1. Diagram of hippocampal anatomy and connectivity. A) 3D model of hippocampal subfields showing subiculum (purple), CA1 (blue), CA2 (cyan), CA3 (green), dentate gyrus (yellow), and dark band (red). B) Cross-section of hippocampal body (red dotted line from A) showing connectivity between subfields. Solid lines denote the indirect pathway, dashed lines denote additional pathways, and dotted line indicates recurrent collaterals within CA3. B) is a modified copy of ‘Stylised diagram of the hippocampus’, Wikimedia Commons: Hippocampus\_(anatomy). See <sup>16</sup> for credit and copyright license details..... 4
- Figure 2. Diagram of steps employed in our hippocampal subfield segmentation protocol. Orange indicates manual steps, whereas blue indicates automated or computational user-guided steps. ‘In development’ refers to work still in progress, with only preliminary results presented in this thesis..... 18
- Figure 3. Manual segmentation and translation of histological characterization of hippocampal subfield by Ding *et al.* <sup>37</sup>. Purple shows the subiculum, blue CA1, cyan CA2, green CA3, yellow dentate gyrus, and red shows hippocampal dark band. A) MRI slice from the hippocampal body (left) and the labelled subfields in that image (right). Arrows indicate potential protocol rules (see text). B) Same structures as A), but in the hippocampal head where the uncus can be seen on the medial side. C) 3D model of all subfields throughout the hippocampus. D) Example hippocampus not separated into subfields, but demonstrating the digitations in the hippocampal head continuing along the lateral and inferior side of the body. .... 29
- Figure 4. Dilation and manual adjustments of dark band to generate hippocampal grey matter volume. A) Dark band trace on individual slice (left), and a 3D model of the dark band (right). B) Dark band is dilated until it reaches the external border of hippocampal grey matter on the inferior, lateral, and superior sides (left), producing a 3D model (right) containing most of hippocampal grey matter. C) Manual adjustments to remove grey

matter label where it was incorrectly labelled and add grey matter label where it was missed. .... 32

Figure 5. Anterior-posterior unfolding of hippocampal grey matter using the Laplacian equation. The anterior-posterior extent of hippocampal grey matter (top left) is labelled with scalars, which are binned into slices (bottom left). Cross-sections along these bins reveal the classic hippocampal ‘C’ shape (right), except in the vertical component of the uncus (bottom right). .... 33

Figure 6. Proximal-distal unfolding of hippocampal grey matter using the Fast Marching algorithm. The proximal-distal extent of hippocampal grey matter (top left) is labelled with scalars, which are binned into strips (bottom left). Slices along the previously described anterior-posterior extent show the labelling within the length of the classic hippocampal ‘C’ shape (right). .... 34

Figure 7. Finished segmentation of two hippocampi: one with many digitations (top) and one with few digitations (bottom). Left models viewed from above and medial, right models from medial and slightly below. Below the models are example coronal slices from the hippocampal body (two left images; with and without subfields imposed) and head (two right images). .... 35

Figure 8. Native MRI voxel intensities across anterior-posterior and proximal-distal gradients. Warm colours indicate high intensities. A) 2D map of normalized voxel intensities. Vertical lines show the subfield boundaries, as mapped onto the 3D model above. The red line indicates the most lateral edge of the hippocampus. B) Subfield models (top) and grey matter model with corresponding voxel intensities mapped onto its surface (bottom) shown from above (left) and below (right). .... 40

# 1. Introduction

The hippocampus is an evolutionarily old brain structure that has a clear homologue in every vertebrate species <sup>1</sup> and that has analogues in species as far down the evolutionary tree as insects <sup>2</sup>. In humans it is a tube-like structure that runs along in the medial temporal lobes, but in animals with less developed temporal lobes such as rodents, it is found superior and posterior to the corpus callosum. The hippocampus is critically involved in cognition and is implicated in a wide variety of neurological and psychiatric conditions. For example, the hippocampus is heavily implicated in Alzheimer's disease, medial-temporal lobe epilepsy, anoxic brain injury, schizophrenia, and depression, as well as other psychiatric disorders <sup>3</sup>. For these reasons, the hippocampus is one of the most extensively studied brain structures in humans and in non-human species. As a result, many structural and functional properties of the hippocampus have been revealed, including that it contains highly plastic neurons <sup>4</sup>, that it is the primary site of adult human neurogenesis <sup>5</sup>, and that it has a highly stereotyped cytoarchitectural organization within its subregions (or subfields). This thesis will discuss and provide and discuss a detailed protocol for the division of the human hippocampus into subfields using *in-vivo* neuroimaging, specifically, structural Magnetic Resonance Imaging. Localizing the subfields of the hippocampus in MRI is not straightforward due to its morphological complexity and limitations in imaging resolution and contrast. However, it does show great promise for understanding pathological changes in conditions that affect the hippocampus, and for uncovering potentially distinct functions of hippocampal components in cognition and behaviour.

## 1.1 Historical context of hippocampal research

While there have been many significant leaps in our understanding of the hippocampus, there is still no dominant unified theory of its function. There are currently two major ideas regarding the function of the hippocampus: spatial navigation and memory. After discovering neurons in the hippocampus of rats that become active in association with a specific spatial location, O'Keefe and Dostrovsky put forth the idea that the hippocampus is able to flexibly represent spatial environments <sup>6</sup>. This theory is hugely popular,

particularly among researchers who study non-human animals. For example, the hippocampi of birds, rodents, and many other species, as well as the analogous mushroom bodies in insects, have been linked to foraging behaviours, specifically the ability to map the locations of food sources or caches <sup>7,8</sup>. In humans, on the other hand, the discovery of severe episodic amnesia following bilateral hippocampal lesions in the famous patient H.M. spurred a highly prolific field of research that has not only focused on navigation, but also the role of the hippocampus in other aspects of cognition, most prominently in episodic and semantic memory <sup>9</sup>. Methodological challenges make it difficult to infer the presence of episodic memories that involve the recollection of spatial, temporal, or emotional context of past experiences in non-human animals, but many studies have shown involvement of the hippocampus in something that resembles this process at the behavioral level and in terms of neural underpinnings <sup>10</sup>. With the advent of non-invasive functional neuroimaging in the 1990s, scientists have also started to study the functions of the hippocampus in behaving human participants. This has led to a richness of new data implicating the hippocampus in many aspects of cognition beyond navigation and episodic memory, including, for example, contributions to perceptual processing <sup>11</sup>, emotional regulation <sup>12</sup>, imagining the future <sup>13</sup>, and the extraction of associative, configural, and semantic information from specific past experiences <sup>14</sup>. Against this background, there is no current consensus to ascribe a single function to this brain structure. Most scientists agree, however, that the hippocampi are key contributors to cognition in almost all species that exhibit behavioural flexibility, at many levels of complexity across species.

More recent approaches to studying the hippocampus have increasingly focused on determining the computations that the hippocampus might contribute to dynamic processing in interactions with structures throughout the brain. This approach is motivated in part by the idea that cognition requires interactions at a macro-scale network level, with focal cortical and subcortical nodes performing computations that contribute to more widely distributed processing. Considering the hippocampus as performing some set of computations, we may be able to understand its contributions to a wide range of behaviours and functions. This might help us to understand why the hippocampus becomes involved in such a wide array of functions, some of which presumably require

overlapping computational demands. Furthermore, if the functions of the hippocampus can be understood at the subfields level then they can be more closely related to the underlying cytoarchitecture that defines the subfields. This could help in bridging research on neural function at the micro-scale network level, typically in non-human animals, with research at the macro-scale network level from non-invasive human neuroimaging studies.

## 1.2 Hippocampal subfield anatomy

The computational approach to studying the hippocampus is motivated by cytoarchitecture and circuitry properties. The hippocampus has been extensively studied using *in-vivo*, *in-vitro*, and *ex-vivo* techniques at the micro-scale, but this knowledge cannot easily be translated into the domain of macro-scale neuroimaging studies. Based on neuroanatomical work, we know that the hippocampus can be divided into subfields with distinct cytoarchitectonic and connectivity profiles. In a seminal monograph on the topic, Duvernoy synthesized information from many studies into a comprehensive description of human hippocampal anatomy and connectivity<sup>15</sup>. At a glance, the hippocampal subfields consist of the dentate gyrus, cornu ammonis (CA) fields 1-3, and the subiculum (which can be further divided into prosubiculum, subiculum proper, presubiculum, and parasubiculum) (see Figure 1). The subiculum is continuous with surrounding medial-temporal lobe cortex (entorhinal and parahippocampal cortex) but it is still considered part of the hippocampal formation. The CA fields are continuous with the subiculum and consist of archicortex, which has a different architecture and laminar structure, and is evolutionarily older than neocortex. Curled medially inside the CA fields is a distinct tissue compartment called the dentate gyrus. The connectivity between these subfields follows two prominent pathways, the direct and the indirect (also called monosynaptic and trisynaptic) pathways, respectively. The direct pathway projects from the entorhinal cortex to CA1, then to subiculum and back to the entorhinal cortex. The indirect pathway projects from entorhinal cortex to dentate gyrus to CA3 to CA1 and then projects back to entorhinal cortex via the subiculum. Additional connections also exist between subfields; for example, some axons originating from the entorhinal cortex bypass the dentate gyrus and synapse directly on CA3, as illustrated in Figure 1b. Finally,

in addition to their primary output via subiculum back to entorhinal cortex, the CA fields additionally send axon projections to the mammillary bodies and anterior thalamic nuclei via white matter structures known as the alveus, fimbria, and fornix. The connectivity profiles of each subfield, as well as observations about their cytoarchitecture, has led to several prominent hypotheses about the computations performed by each of these structures.

In a coronal section of the hippocampus, the arrangement of these subfields consistently follows a ‘C’ shape arrangement in much of the hippocampus (Figure 1b). However, in the anterior and posterior ends of the hippocampus, often known as the hippocampal head and tail respectively, the hippocampus curves medially (Figure 1a). The medial portion of the hippocampal head, known as the uncus, often curves posteriorly and then upwards as well. Despite these complexities, the subfields of the hippocampal head and tail show the same connectivity and similar cytoarchitecture as their counterparts in the hippocampal body<sup>15</sup>.

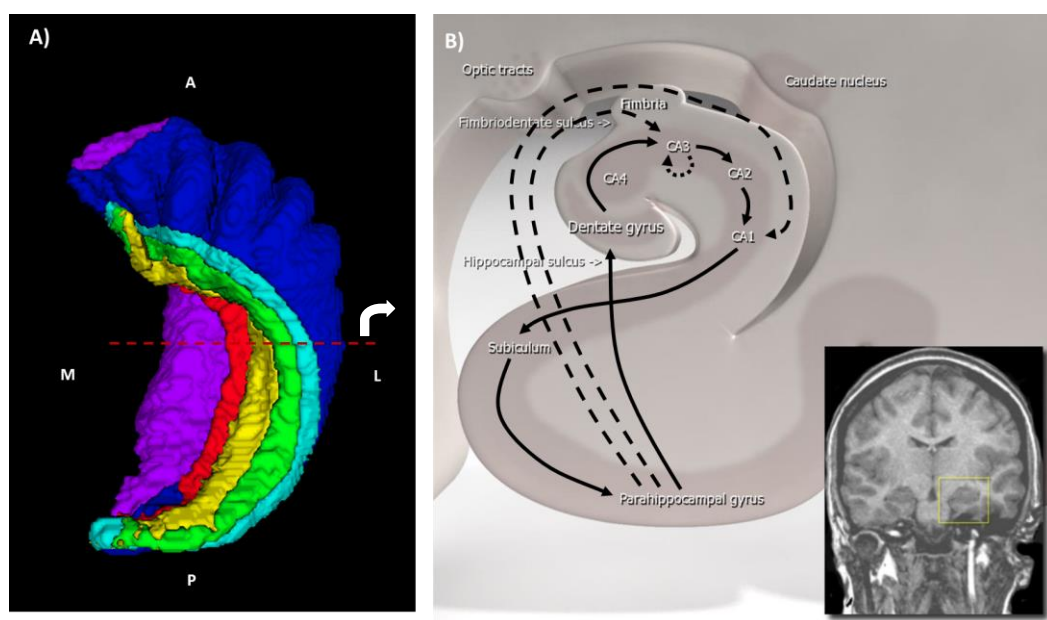


**Figure 1. Diagram of hippocampal anatomy and connectivity. A) 3D model of hippocampal subfields showing subiculum (purple), CA1 (blue), CA2 (cyan), CA3 (green), dentate gyrus (yellow), and dark band (red). B) Cross-section of hippocampal body (red dotted line from A) showing connectivity between subfields.**

**Solid lines denote the indirect pathway, dashed lines denote additional pathways, and dotted line indicates recurrent collaterals within CA3. B) is a modified copy of ‘Stylised diagram of the hippocampus’, Wikimedia Commons: Hippocampus\_(anatomy). See <sup>16</sup> for credit and copyright license details.**

### 1.3 Subfield-specific computational accounts of hippocampal function

To illustrate a proposed mapping of specific computations on distinct hippocampal subfield cytoarchitectures, it is informative to focus on computations referred to as pattern separation and pattern completion in the neuroscience literature <sup>17</sup>. Pattern separation reflects the orthogonalization of overlapping inputs into highly distinct outputs, and this can be achieved by taking potentially overlapping inputs and spreading them over a much larger population of cells. By doing this, any subtle differences in the input pattern will be amplified in the output pattern. Unlike the other hippocampal subfields, the dentate gyrus is a distinct tissue composed mainly of a dense layer of granule cells. These granule cells are organized largely in parallel, with inputs on one side from a comparatively small population of entorhinal pyramidal cells, and outputs on the other side to the CA fields (indirect hippocampal pathway). This lead Marr to propose that the dentate gyrus performs pattern separation via expansion recoding <sup>18</sup>. His proposal has gained a lot of traction over recent years, and evidence for pattern separation in the dentate gyrus has been collected using a wide range of techniques and experimental designs (see <sup>19–22</sup>). It has also been suggested that pattern separation is particularly advantageous when trying to encode a new episodic experience. Many elements of episodic experiences are often shared with other events, but we are still able to maintain unique representations of similar experiences. This characterization also fits well with the dentate gyrus’ position in the indirect hippocampal pathway: pattern separated information about an ongoing event is passed from the dentate gyrus to the CA fields, and modification to the synapses on the CA fields and from the CA fields onward might ultimately support a highly distinctive long-term episodic memory.

The complementary operation to pattern separation is pattern completion. It reflects the retrieval of a stored representation given only a partial or degraded cue. In a prominent

proposal, this computation has been ascribed to CA3, which has a high number of recurrent collaterals (Figure 1b) making it well suited to act as an autoassociative attractor (see <sup>23</sup>). This means that the attractor (the CA3 in this case) will recurrently modify its activity until it reaches some stable state. The stable state will depend on the inputs from which the attractor started, as well as its previously structured internal connections. With small to moderate changes in the input signal, the attractor will still produce the same output (i.e. completing the pattern that was present at encoding). However, beyond some threshold of changes to the input, the autoassociative attractor will begin to form other states and thus produce a large difference in output. Evidence for this computation in the CA3 has been seen in a large set of studies, and is most closely associated with the retrieval phase of episodic memory <sup>17–22</sup>. Furthermore, the CA3 receives some direct input from the entorhinal cortex (i.e. bypassing the dentate gyrus), which may engage the automatic generation of potentially matching CA3 states, even to a completely novel input pattern. This could be adaptive in guiding our predictions or even helping us to select a template through which we might understand and encode an episode <sup>24</sup>. Pattern separation and pattern completion may be involved in a wide array of functions beyond their roles in episodic memory. For example, hippocampal pattern separation and completion have been implicated in real-time navigation and perceptual discrimination. In navigation, selection of the correct memory of the layout of an environment among competing, highly similar memories may rely on both hippocampal pattern separation and completion <sup>25</sup>. In perception, hippocampal pattern completion may help guide predictions about a visual stimulus <sup>26</sup> while pattern separation may facilitate discrimination of highly similar stimuli (as discussed by <sup>11</sup>).

## 1.4 Techniques for imaging the human hippocampal subfields

The hippocampus is easily imaged structurally and functionally as a whole entity. However, obtaining specificity at the level of hippocampal subfields requires highly focused imaging approaches. Commonly used T1-weighted MRI and high-resolution fMRI are typically not sensitive to distinctions between such small structures because of their relatively large voxel size.

The development of MRI techniques that allow for visualization and characterization of the hippocampus at the subfield level have received an increasing interest in recent years. An overwhelming majority of developers of segmentation protocols agree that T2-weighted images are best for performing segmentation, as opposed to T1-weighted images which are more commonly used in whole-brain structural imaging in current research <sup>27</sup>. This is in part due to the availability of a key landmark that can be visualized most easily in T2-weighted imaging: the hippocampal ‘dark band’ <sup>28-31</sup>. The dark band is thought to be composed of high myelin strata of the CA fields and dentate gyrus - stratum radiatum/stratum lacunosum/stratum moleculare (SR/SL/SM; also abbreviated to SRLM or SLM) <sup>28-31</sup>, and is often used as a key landmark in locating hippocampal subfields. In addition to weighting, resolution and signal-to-noise ratio in an image will limit features that are available for segmentation.

In-vivo imaging limits the time that participants can be scanned. That is, the scans are conventionally limited to less than 10 minutes to prevent participants from becoming uncomfortable or moving around, which creates severe artifacts in an image. However, some interesting techniques have recently been developed to gain greater signal-to-noise and higher resolution using equivalent scan times. One advance involves acquiring data over the volume of the hippocampus only, in coronal-oblique orientation to the hippocampus while maximizing in-plane resolution and taking relatively thick slices (or between-plane resolution) <sup>27</sup>. This approach takes advantage of the observation that the hippocampal body (i.e. the midsection along its anterior-posterior length) has a relatively constant subfield structure perpendicular to this plane. High in-plane resolution allows for the viewing of relatively small structures inside the hippocampus, like the dark band. However, the head and tail of the hippocampus both curve medially, and the head of the hippocampus even extends back along its own length before then curling upwards <sup>15</sup>. This anatomical feature implies that in these regions the subfields of the hippocampus will run across the thick slices, such that image acquisition essentially involves averaging of signals across borders of interest. It also reduces the visibility of the hippocampal dark band in the head and tail, leading to reduced availability of critical information within the hippocampus to guide segmentation. Nonetheless, this technique is still the most popular method for image acquisition among current subfield segmentation protocols <sup>27</sup>.

Another MRI technique for optimization of subfield segmentation involves acquisition of multiple high-resolution scans that each have relative low signal-to-noise, and then co-register and average these images to recover better signal-to-noise<sup>28</sup>. It is possible to algorithmically upsample the individual scans before co-registration to further enhance alignment (e.g.  $0.6\text{mm}^3$  isovoxels resampled to  $0.3\text{mm}^3$  will produce better coregistration in cases where movement between scans was off by a factor of  $0.3\text{mm}^3$ ), which has been shown to significantly improve image quality<sup>28</sup>. Finally, other recent protocols have employed ultra-high field strength MRI for subfield imaging of hippocampal subfields (i.e. 7-Tesla MRI). Use of ultra-high field strength imaging increases the signal-to-noise ratio of images in an equivalent amount of scan time, and allows for acquiring volumes at higher resolution (e.g.<sup>31,32</sup>).

## 1.5 Techniques for segmenting hippocampal subfields in MR images

The defining feature of each hippocampal subfield is its cytoarchitecture. However, current MRI techniques do not allow for *in-vivo* imaging at the cellular level. Accordingly, the borders between subfields cannot be easily identified in a structural scan. Given the promise of examining the hippocampus at a subfields level, many researchers have tried to overcome this problem by estimating these borders indirectly. Yushkevich *et al.* recently provided a systematic comparison of 21 protocols for subfield segmentation to assess the level of detail and precision, the basis for determining borders, and the agreement between segmentations performed by various groups on the same dataset<sup>27</sup>. This work represents an effort to identify current challenges and to harmonize the various protocols for subfield segmentation towards use a single consensus protocol, which would allow for easier comparison of results across studies at the subfields level.

Broadly speaking, development of subfield tracing protocols is obtained by making reference to anatomical landmarks that can be seen in MRI (some of which are within the hippocampus, and some of which are based on surrounding structures), and introducing geometric rules to describe subfield locations in relation to those landmarks (e.g. a border lies at most lateral point in the hippocampus, or halfway in between two other visible structures). These landmarks and rules are typically identified based on *ex-vivo*

histological staining of hippocampal tissue, which allows researchers to detect microscopic cytoarchitectural differences that define the subfields (a representative protocol can be found in <sup>30</sup>). By far the most popular choice for histological reference images is Duvernoy's seminal monograph that offers a synthesis of extant knowledge about hippocampal anatomy and vascularization at the time of its publication <sup>15</sup> (used in 16 protocols discussed by <sup>27</sup>). Thus, by aligning structures that are visible in an MR image with structures in an *ex-vivo* sample, researchers can predict where the borders of subfields will be in the MR image and describe their morphologies with respect to visible image features. This is typically done on a slice-by-slice basis following coronal slices, given that on such slices the hippocampus follows a fairly consistent 'C' shape coronally throughout much of its body. With this consistency, a relative simple set of rules can be used to describe subfield borders to a reasonable degree of accuracy and with good reliability (although, see section 1.5 below). The hippocampal head has a far less consistent arrangement of subfields between slices, and as a consequence reliability and accuracy of subfield tracing is typically significantly lower here <sup>27</sup>.

An additional technique used by some researchers involves acquiring very high quality data from *ex-vivo* tissues in 9.4T scanners, performing the best possible subfield segmentation, and then translating the results to more widely available, lower resolution image (e.g.<sup>33</sup>). This translation can involve downsampling and coregistration of data with lower resolution images, or manually choosing subfield borders in lower resolution images by comparison with finer segmentation from the *ex-vivo* tissue. In the *ex-vivo* imaging data, many more image features are available and histological information on subfield locations can be carried to the MR images with greater precision.

## 1.6 Challenges and limitations in current subfield tracing protocols

Yushkevich *et al.*'s recent survey of subfield tracing protocols <sup>27</sup> revealed that there is currently substantial disagreement between labs as to where each border should be drawn, and even as to what labels should be used to describe the arrangements of subfields. This is in part because of the different histological reference materials used by different labs, as morphological variations in the hippocampi used as references will

create discrepancies in tracing protocols. An effort is currently being made by a group of investigators from several laboratories, called the Hippocampal Subfields Group (HSG), to consolidate this wide set of rules and reference materials into a single harmonized protocol (<http://www.hippocampalsubfields.com>). Given that the body of the hippocampus contains the most consistent arrangement of subfields, work in this group started by focusing on harmonizing protocols for tracing the body as a first step. However, it should be noted that there is a significant amount of inter-individual variability in morphology, which is not always captured by protocols that use rigid rules and landmarks for segmentation. This represents a major issue for a harmonized protocol that is based on gross anatomical landmarks and rules rather than subfield-specific cues in MRI.

The HSG has acknowledged that the hippocampal head and tail present a particular challenge for subfield segmentation, and more research is required before a harmonization of protocols for these areas can be completed. This is in part because of MR imaging constraints, but also because the spatial relationships between subfields become much more complex in the hippocampal head. Some existing protocols for segmentation have simplified the hippocampal head by giving it ambiguous labels, for example by combining many subfields into a single label, or providing a single label for the entire hippocampal head without further division. Other protocols have tried to follow the complex morphology of subfields but, due to lack of available features in their images and lack of literature on the hippocampal head, have misrepresented subfield structure<sup>27</sup>. Some common errors that can be seen in the protocols discussed by Yushkevich *et al.*<sup>27</sup> are that the superior side of the medial hippocampal head is often labelled entirely as CA1, whereas in reality all of the subfields are present in this area. This represents a major issue given that the hippocampal head represents roughly half of the geodesic length of the hippocampus<sup>15</sup>. Another common error is that the digitations in the hippocampal head are not accounted for, and so the dark band that separates the dentate gyrus from other subfields is misplaced. This is especially problematic because it profoundly affects the thickness and overall volume of each of these subfield labels.

Manual subfield tracing protocols require subjective and labour-intensive implementation by an expert. This leaves room for subjective judgments as to where landmark structures begin or end, and what tissue reflects hippocampal grey matter as opposed to CSF or white matter. The latter can often be difficult to determine in a single plane of view. Some researchers have tried to use tools that can operate on data in 3D rather than in 2D slices to solve these problems. One popular choice is the automated segmentation offered in the Freesurfer software package <sup>34</sup>. However, this pipeline uses standard T1-weighted images from 1.5- or 3-Tesla scanners and is not able to leverage structural features inside the hippocampus <sup>35</sup>. Many similar pipelines have been developed, but most appear to be based on the overall volume of the hippocampus rather than subfield-specific features. One automated technique that has shown particular promise, and which operates on data where intra-hippocampal features like the dark band are available, is ASHS - Automated Segmentation of Hippocampal Subfields <sup>32,36</sup>. Until recently, this pipeline did not segment the head or tail of the hippocampus because of their complex structure. With its latest release, ASHS does segment the entire length of the hippocampus, but critically, it does so based on data from a large number of manual segmentations. This means that systematic errors or simplifications of subfield morphology in manual traces will be carried forward into automatically segmented hippocampi.

## 1.7 Recent advances in knowledge of subfield anatomy

Recent evidence from histology in human hippocampi has emerged that promises to offer information that could lead to further improvement of MR-based subfield protocols <sup>37</sup>. Specifically, Ding *et al.* offer a new morphological characterization of the hippocampal head, the part of the hippocampus that is most difficult to segment due to its complex shape and folding. This study examined densely sampled coronal slices along the length of the hippocampal head in several different *ex-vivo* specimens. The authors emphasize that the digitations (i.e. folds) in the hippocampal head differ considerably across individuals, varying from 2 to 5 digitations. They recommend using these digitations for alignment of the coronal slices documented in their histological study to coronal slices obtained with MRI in order to help identify subfields and to account for additional inter-individual differences.

Ding *et al.*<sup>37</sup> also note that all of the hippocampal subfields are present in the uncus- a part of the hippocampal head that curves medially and then runs slightly backward along its own longitudinal axis before curving upwards. As the subfields curve into the uncus, their borders also shift such that in the very anterior portions, the subiculum moves from a position on the inferior side, as in the body of the hippocampus, to a position that wraps around the lateral superior sides. Furthermore, Ding *et al.* showed that all the subfields of the hippocampus, including the subiculum, contiguously follow this curvature through the hippocampal head and have their natural anterior termination not in the anterior end of the hippocampus, but rather in the more medial and posterior vertical (i.e. upward curving) component of the uncus. A quick examination of segmentation models in Yushkevich *et al.*'s comparison of protocols shows that no protocol honours this pattern<sup>27</sup>. To our knowledge, this recent evidence has not yet been translated into an MR-based subfield tracing protocol, but it presents a promising avenue for improvement.

## 1.8 Structural and developmental regularities

In order to understand the complex morphology of the hippocampal head and develop protocols that allow for accurate subfield segmentation, it can be informative to consider changes in ontogenetic development of the hippocampus. During development, the hippocampus originates from a single flat tissue, which then folds upon itself while differentiating into the various subfields<sup>15,37</sup>. This developmental characteristic has several interesting consequences for the structure of the adult hippocampus: all subfields, except the dentate gyrus that breaks off to form a distinct tissue during development, make up adjacent segments of a contiguous tissue segment. As a consequence, there are consistently preserved spatial relationships between subfields. The contiguous tissue segment wraps around the dentate gyrus, forming a classic 'C' shape, which, as previously mentioned, can be seen in cross sections throughout the hippocampal body. Furthermore, blood vessels running along the surface of the flat tissue from which the hippocampus originates get confined to the vestigial hippocampal sulcus, i.e., the space in between the folds of hippocampal grey matter (see Figure 1b). Interestingly, these blood vessels also coincide with the hippocampal dark band seen in MRI, and would appear dark in T2-weighted images. This introduces the possibility that the dark band is made up

of blood vessels in addition to high-myelin laminae, or SRLM, as described above. If true, this might suggest the dark band is not reliable as a landmark. However, the blood vessels necessarily fall within the vestigial hippocampal sulcus which is in turn surrounded by the SRLM and so the dark band is still likely to fall in a consistent position in MRI and can act as a reliable landmark. The dark band is surrounded on the outside by the CA fields, and on the inside by the dentate gyrus. In fact, the only part of the hippocampus that does not directly contact the dark band is the subiculum, which extends medially past the vestigial hippocampal sulcus and does not contain the high-myelin laminae of the CA fields (the SRLM). Thus, we propose that the dark band can be useful for gaining information about where its surrounding subfields should fall.

As well as forming a ‘C’ shape in cross-sectional planes, the tissues of the hippocampus are also curved in the anterior-posterior direction (see Results Figure 2b; also recently discussed by <sup>38</sup>). The tail of the hippocampus curves medially, and the head of the hippocampus curves medially, posteriorly (running slightly backward along the longitudinal axis of the hippocampus), before also curving upwards. A protocol for segmenting the hippocampal head in detail must reflect these various types of curvature, showing all subfields curving medially into the different components of the uncus.

Finally, as mentioned above, each of the hippocampal subfields contains a unique cytoarchitecture. This is achieved during development through the differential modification of regions along the length of what was originally a flat tissue (before its folding during development). It differentiates the grey matter of the hippocampus, sometimes referred to as archicortex, from neighboring medial temporal-lobe neocortex. The cytoarchitecture is also what differentiates the subfields within the hippocampus <sup>15</sup>, but to date no tracing protocol has been based on any visible differences between grey matter in these different subfields. Nevertheless, it may be possible to make related predictions for differences in image intensities on very high signal-to-noise and ultra-high resolution MR images based on myelin content, as documented in Duvernoy’s work <sup>15</sup>. The perforant path consists of axons passing from the entorhinal cortex to the dentate gyrus, and makes up the primary input pathway to the hippocampus. This pathway passes through (or ‘perforates’) the grey matter of the subiculum. Accordingly, one might expect

that the subiculum display some stronger resemblance to high-myelin white matter (dark in T2-weighted images) as compared to the other subfields. The other subfields send most of their axon projections through the high myelin laminae in the hippocampal dark band and through the alveus, a thin lamina of white matter that surrounds much of the hippocampus before converging into a bundle known as the fimbria and leaving the hippocampus via the fornix. Given their spatial position, these axons likely do not influence the intensities of hippocampal grey matter in other subfields. However, as mentioned above, the CA3 has a high density of recurrent collaterals composed of axons that terminate on the neurons they originate from, as well as on neighbouring neurons<sup>15</sup>. This feature may lead to an overall greater density of myelin within the grey matter of CA3. CA2 is the most vascularized subfield in humans, closely followed by CA3 and in contrast with the limited vasculature in CA1. These differences in vascularization may be reflected in darker intensities in areas CA2 and CA3, with lighter intensities in CA1. Finally, the dentate gyrus consists of a large number of granule cells whose tightly packed cell bodies might increase the local water content. As a consequence, the dentate gyrus may appear brighter than other subfields in T2-weighted images. These types of predicted intensity differences have not been leveraged or even described in any manual tracing protocol that we know of to date<sup>27</sup>, perhaps because they are not consistently noticeable on individual slices even at ultra-high image resolution. Here, we explored their potential value for segmentation, hypothesizing that corresponding differences in image intensity might be observed when large areas of hippocampal grey matter are considered in combination with knowledge about the continuities in spatial relationships between subfields.

## 1.9 Goal of the current study

In the current study we aim to develop a new protocol for the segmentation of the subfields of the hippocampus, taking into account the known complex curvature and digitations (i.e. folds) in the hippocampal head. We aim to overcome the limitations of previously published protocols by taking advantage of advances in structural MR imaging techniques that include (i) image acquisition at ultra-high field strength (7-Tesla); (ii) use of multiple repeated image acquisitions with upsampling and averaging

between scans, and (iii) the use of isotropic voxels to improve visibility of small structures in the medially curving head and tail of the hippocampus. With this combined set of optimizations, we aim to implement newly available histological information about the morphology of the hippocampal head as reported by Ding and colleagues<sup>37</sup>, paying special attention to the continuous nature of hippocampal subfields throughout the curvatures that characterize the hippocampal head and uncus as a result of its ontogenetic development. Towards this end, we plan to use a mixture of manual and semi-automated tools for segmentation of hippocampal subfields that are centered on the detection of the hippocampal dark band, and that are informed by potential differences in image intensities that may come about as a result of differences in cytoarchitecture. For initial assessment of the quality of this protocol, we also plan to assess inter- and intra-rater reliability of finished segmentations, similarly to other manual segmentation protocols.

## 2 Methods

This section presents the methods used for the development of our hippocampal subfield segmentation protocol, the protocol itself, and then the methods used to assess reliability of our protocol.

### 2.1 Participants

Healthy subjects were recruited from Western University, London, Canada ( $n = 12$ ; 6 females; ages 20-35, mean age 27.6). This study was conducted with Western's Human Research Ethics Board approval.

### 2.2 Image acquisition

Imaging was performed on a 7T neuroimaging optimized MRI scanner (Agilent, Santa Clara, CA, USA/ Siemens, Erlangen, Germany) using a 16-channel transmit-receive head coil array constructed in-house. Four T2-weighted TSE 3D (3D sagittal, matrix:  $260 \times 366$ , 266 slices,  $0.6\text{mm}^3$ ) images were acquired from each participant. Note that by using isotropic voxels, we are able to capture small features such as the hippocampal dark band or other subfield boundaries in high detail, even when they are parallel to the orientation of image acquisition (which is often the case in the hippocampal head). A T1-weighted MPRAGE (3D sagittal, matrix:  $256 \times 512$ , 230 slices,  $0.59 \times 0.43 \times 0.75\text{mm}^3$ ) scan was also collected, but these data were not used in segmentation.

### 2.3 Preprocessing

Preprocessing included motion correction and upsampling of T2-weighted images to  $0.3\text{mm}^3$  isovoxels and then rigid registrations of scans 2, 3, and 4 to scan 1. All four scans were then averaged together to produce a single,  $0.3\text{mm}^3$  isovoxel, high-contrast volume. This technique of upsampling and then coregistering and averaging multiple scans allows for a closer coregistration of images, and has been shown to improve contrast-to-noise<sup>28</sup> (see Introduction section 1.3). Manual segmentation of the dark band and then subsequent dilation and adjustments were carried out on the same images after they had undergone standard FSL5.0 FAST preprocessing including intensity

normalization and bias field correction<sup>39</sup>. This made some computational tools easier to use - otherwise the very high intensities of CSF in the ventricles would cause the rescaling of desired contrast and edge-attraction parameters to ranges that don't correspond to borders around hippocampal grey matter. All subsequent analyses were carried out in the four-averaged and coregistered scans only (i.e. no FSL preprocessing). All manual tracing and user-guided computations were performed in ITK-SNAP 3.4<sup>40</sup>.

## 2.4 Generation of reference hippocampal models

In order to have a reference model of the hippocampal subfields to which we could compare subsequent segmentations generated from our protocol, we performed fully manual and highly detailed segmentation of two representative hippocampi. This work was a direct manual translation of the descriptions of hippocampal subfield anatomy from the histological study of the hippocampal head of Ding *et al.*<sup>37</sup>. Specifically, this was done by first tracing the entire hippocampus using the recently harmonized protocol for whole hippocampus volumetry<sup>41-44</sup>. Then, for each coronal slice in an MRI volume, we found the closest corresponding slice in Ding *et al.*'s study and relabeled voxels according to their corresponding subfield in the *ex-vivo* histology. Ding *et al.* point out that different hippocampi can have 3 to 5 digitations in the hippocampal head, and provide histological slices or schematic diagrams of subfield locations in representative hippocampi with 3, 4, or 5 digitations separately. Ding *et al.* also suggest that the digitations may be large enough to be seen in MRI, and so might provide a useful landmark for a segmentation protocol for the hippocampal head. With this in mind, manual segmentation was performed on one hippocampus with 5 clear digitations, and one with only 3 clear digitations, and histological slices from hippocampi with the same number of digitations were used as reference for segmentation. In the hippocampus with 5 digitations, segmentation was performed along the entire length of the hippocampus, using Duvernoy's description of subfields for the body and tail of the hippocampus<sup>15</sup>. In the hippocampus with 3 digitations, only the head of the hippocampus was segmented in detail. Labels included were dark band, dentate gyrus, CA3, CA2, CA1, subiculum, and hippocampal cysts. Dark band and hippocampal cysts were labelled not where they appear in the histology, but rather where they were visible in the MR image. Ding *et al.*

further subdivide the subiculum, but as an initial effort we gave it a single label to try to keep our protocol as simple as possible. Manual tracing was performed in ITK-SNAP using the paintbrush tool. 3D models of the subfield morphologies were generated using the same software. See Results section 3.1 and Figure 2.

## 2.5 Overview of segmentation protocol

We developed a user-guided, semi-automated protocol for segmenting the subfields of the hippocampus that could optimally make use of available image features as well as prior knowledge about hippocampal anatomy and ontogeny. This involved the following 7 steps: (i) manual tracing of the hippocampal dark band; (ii) dilation of the dark band label to efficiently detect the majority of hippocampal grey matter; (iii) manual adjustments to the hippocampal grey matter label and extra-hippocampal labels; (iv) computational unfolding and indexing of hippocampal grey matter along its anterior-posterior axis; (v) computational unfolding and indexing of hippocampal grey matter along its proximal-distal axis; (vi) definition of borders that best match Ding *et al.*<sup>37</sup> and our previously generated reference models using anterior-posterior and proximal-distal indices; and (vii) application of these borders to hippocampal grey matter in native MRI space (Figure 1). We also present preliminary results for ongoing work to improve the definitions of subfield borders in the unfolded hippocampal grey matter tissue.

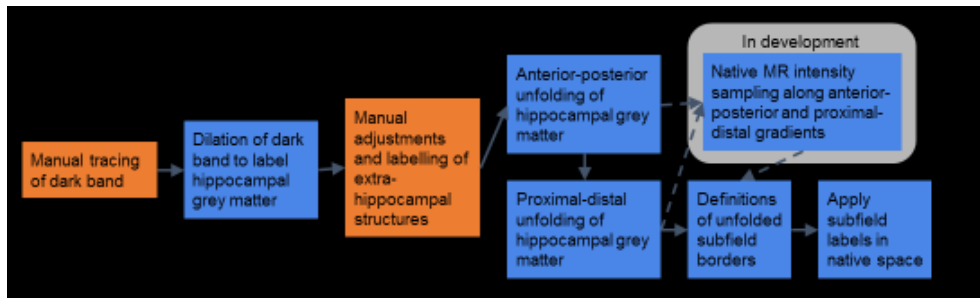


**Figure 2. Diagram of steps employed in our hippocampal subfield segmentation protocol. Orange indicates manual steps, whereas blue indicates automated or computational user-guided steps. ‘In development’ refers to work still in progress, with only preliminary results presented in this thesis.**

The hippocampal dark is an image feature that appears dark compared to surrounding grey matter in T2-weighted images. Given our highly specialized MR acquisition protocol, this feature was visible in the entire anterior-posterior extent of the hippocampus. The band makes up a continuous, thin structure adjacent to each of the other subfields except the subiculum. Much of the morphology of the hippocampus can be determined by looking at a model of the dark band alone (e.g. number and locations of digitations; curvature of the uncus and tail) (see Results section 3.1 and Figure 3). Because the dark band consists of the innermost laminae of the CA subfields and encircles the dentate gyrus, it necessarily must border each of these tissues. If the dark band is indeed also made up of blood vessels, as we suggest following an examination of Duvernoy's monograph, we know that the folding of the hippocampus during development means that these blood vessels must follow the path of the vestigial hippocampal sulcus which itself borders the innermost laminae of the CA fields and encircles the dentate gyrus. Thus although we are still not certain which tissues contribute to the appearance of the dark band, we can be confident that it will consistently be perpendicular and adjacent to the CA fields and dentate gyrus. The dark band is the most prominent intra-hippocampal feature in our MR images, so we reasoned that it could be traced with a high degree of reliability. Tracing of the hippocampal dark band corresponds to step (i) in section 2.5 and is detailed in Appendix A.

## 2.6 Hippocampal grey matter

The various subfields of the hippocampus develop from a single, thin, folded tissue consisting of a modified cortex (archicortex). Thus we anticipated that the subfields might each have a relatively consistent, preserved thickness after we take into account their folding. This is not necessarily the case, as modification of the subfields during development that causes them to take on their unique cytoarchitecture could also lead to increases or decreases in thickness in some subfields more than others. However, we attempted to make use of the assumption that the thickness would not vary too much to facilitate segmentation, and later introduced additional measures to allow the subfields to vary in thickness depending on the MR image.

We tested whether we could recover the shape of the entire hippocampus (i.e. hippocampal grey matter that makes up each of the subfields) by tracing and then dilating the hippocampal dark band label. We performed supervised morphological dilation of the dark band in order to label the surrounding grey matter of the hippocampus. For this, we used ITK-SNAP's Snake tool <sup>40</sup>, which evolves a seed region in 3D to fill a structure of interest. This tool can be constrained by intensity thresholding or edge attraction information, which are applied to an image after some transformations such as selected intensity ranges or spatial smoothing. The parameters of the image transformation and the parameters of the evolution are interactively chosen by the user. These constraints determine the way in which a seed region will iteratively evolve until stopped by the user. In our case, we initialized the evolution using the dark band and applied no constraints on the evolution, resulting in uniform, spherical dilation of the label. The amount of dilation was determined by visually inspecting whether the outer borders of hippocampal grey matter had been reached, and varied slightly depending on the volume of the hippocampus being traced.

In order to allow the different parts of hippocampal grey matter to vary in their thickness, we performed some edge attraction to the outer border of the hippocampus using ITK-SNAP's Snake tool <sup>40</sup>. Smoothing, intensity selection, and other parameters were chosen by the user to best suit the MR image being segmented. This must typically be done manually by an experienced segmenter, and corresponds to step (ii) in section 2.5. It should be noted that some borders of the hippocampus are more high-contrast and lower spatial frequency than others, depending on whether there is white matter, CSF, or small structures such as the alveus, blood vessels, or choroid plexus on the outer borders of the hippocampus. For this reason, there are no edge attraction parameters that will capture all borders. Only the lateral, superior and inferior borders can typically be fitted like this, and the medial and sometimes superior border must be adjusted manually. For this reason, we introduced a set of manual adjustments to fill in hippocampal grey matter that was missed and remove label that was erroneously dilated outside of the hippocampus. In particular, no dark band can be seen running overtop of the subiculum or the vertical component of the uncus, so the grey matter comprising these structures has to be filled in

manually. This step corresponds to (iii) in section 2.5. Detailed instructions for dilation of the dark band and the subsequent manual adjustments are described in Appendix A.

## 2.7 Computational techniques for dealing with convoluted tissues

Because of the ontogeny of hippocampal grey matter, its fully developed structure still consists of an entirely continuous but highly convoluted tissue, not unlike the neocortex. In the neocortex, 3D computational tools have been developed that can flexibly take into account the highly folded morphology when calculating other properties of grey matter tissue. For example, the Laplacian equation has been used to calculate neocortical thickness<sup>44</sup>. In principle, the technique generates a scalar field, or gradient, where the values range from 0 to 1 depending on their distance from two boundaries (often called source and sink). In calculating neocortical thickness, the source can be defined as the white matter below the neocortex, the sink is the CSF outside of the neocortex, and a gradient is generated over the grey matter of the neocortex. If the source is given a value of 1, and the sink a value of 0, then all voxels in neocortical grey matter are given a value between 0 and 1 corresponding to their distance from either boundary (see Appendix 2a for mathematical definition). Streamlines can then be generated from this vector field, and the length of those streamlines will accurately represent cortical thickness even in areas of very high folding.

Another similar method called Fast Marching has also been used in computing cortical thickness while accounting for the many convolutions of the cortex<sup>45</sup>; see also<sup>46</sup>. In principle, the Fast Marching method walks outward from a starting point or set of points, labelling the points it passes by with their distance (or rather, the time it would take to reach that point while travelling at a given speed) from where it started<sup>47</sup> (see Appendix 2b for mathematical definition). Thus in calculating cortical thickness, only one starting point has to be defined (e.g. the white matter beneath neocortex) and all voxels in an image will be assigned a value corresponding to their distance from that point. By extracting values only in grey matter, streamlines corresponding to cortical thickness can again be computed as in the Laplacian technique.

We were inspired by the effectiveness and flexibility of these techniques, and so we attempted to apply them to hippocampal grey matter to ‘unfold’ its structure (or rather, index grey matter in a way that accounts for its folding and curvature).

## 2.8 Unfolding of hippocampal grey matter along anterior-posterior axis

Along its longitudinal axis, grey matter in the hippocampus folds to form digitations, and curves medially, posteriorly, and then upward forming the uncus (and vertical component of the uncus). This curvature is a major part of why the subfields of the hippocampal head do not fall in consistent positions between coronal slices, and why the hippocampal head is so challenging to correctly segment. We thus reasoned that accounting for this curvature may provide a framework for defining hippocampal tissue that preserves the consistent relationships among the subfields. Each of the subfields follows the curvature in the hippocampal head and tail, and therefore has its natural terminus not in the most anterior of the hippocampus but rather in the more medial and posterior uncus (specifically, the vertical component of the uncus). Hippocampal grey matter borders the grey matter of the amygdala in the vertical component of the uncus, where there is an area of uncertainty between hippocampus and amygdala typically referred to the hippocampal-amygdalar transition area (HATA). At the tail of the hippocampus, a structure called indusium griseum (which is actually an extension of the dentate gyrus) extends posteriorly from the hippocampus and then upward and anteriorly along the midline of the brain just above the corpus callosum before merging into the cingulate cortex. Manually labelling both these structures is included in step (iii) of section 2.5, and manual instructions for tracing can be found in Appendix A.

The HATA and the indusium griseum make up natural anterior and posterior termini for each of the hippocampal subfields. We sought a technique that could index hippocampal tissue not along its absolute anterior-posterior distance, but rather along its pseudo-geodesic (i.e. not truly geodesic since it is not distance along a surface but rather within a thin, convoluted volume) anterior-posterior extent (i.e. accounting for the folded and curved tissue such that the most ‘anterior’ point would be in the vertical component of the uncus). To this end, we applied the Laplacian equation, using the HATA as a source

and the indusium griseum as the sink. The scalar field over which we wanted to calculate distance from each structure was defined as the grey matter of the hippocampus, and voxels outside of this structure were excluded to effectively insulate the path along which the gradient would be calculated (i.e. the gradient must pass within the folds of each digitation and not between them). We implemented the Laplacian equation in MATLAB by setting HATA voxels to a value of 1000, indusium griseum voxels to a value of 0, and initializing grey matter voxels with a value of 500. We then applied a 3D averaging filter to all voxels in hippocampal grey matter. We repeated this filtering with 50 000 iterations while redefining voxels of HATA and indusium griseum to 0 and 1000 respectively, such that a smooth, stable gradient along hippocampal grey matter was produced. 50 000 iterations was sufficient given the size of the hippocampus and our voxel size, but we subsequently found that initializing the grey matter gradient using the Fast Marching algorithm (as in the next section) could reduce the number of iterations required by a factor of 10. The result is a smooth, pseudo-geodesic gradient that indexes hippocampal grey matter while taking into account its folding and curvature. This step corresponds to (iv) in section 2.5, and is fully automated.

Another interesting feature of the Laplacian equation is the isopotential along the resulting gradient, or a set of scalar points with equal values. In our example, this will correspond to a slice through the hippocampus perpendicular to the anterior-posterior gradient, or in other words, perpendicular to the curvature in the hippocampal head and tail. With this slicing we might expect to recover the classic folded ‘C’ shape of hippocampal subfields along the hippocampal head and tail.

## 2.9 Unfolding of hippocampal grey matter along proximal-distal axis

Each hippocampal subfield is present along the entire pseudo-geodesic anterior-posterior extent of the hippocampus, with the borders between subfields perpendicular to this axis. Thus, we aimed to develop a technique that could produce an indexing gradient that could be applied on a proximal-distal axis (axis named proximal-distal as in <sup>48</sup>; proximal is the border of the subiculum with neighbouring medial-temporal lobe cortex or at the bottom of ‘C’ shape that the subfields form (see Appendix A), whereas distal is the

dentate gyrus or the top/inner part of the ‘C’ shape). We defined the proximal border of the subiculum as the point at which it contacted the grey matter of neighbouring medial-temporal lobe cortex. We could then apply the same sort of Laplacian filtering across hippocampal grey matter by using the border with medial-temporal lobe cortex as the source, but without already tracing the dentate gyrus we had no structure to define as the sink. Thus we instead made use of the Fast Marching algorithm, using a MATLAB toolbox called Fast Marching toolbox (based on <sup>47</sup>). We defined the border of hippocampal grey matter with medial-temporal cortex as the starting point, and to insulate the path which the Fast Marching would take, we gave hippocampal grey matter voxels low resistance (0.01) and all other voxels high resistance (1.00). This ensured that the resulting gradient would denote the shortest path through only hippocampal grey matter (i.e. pseudo-geodesic) to the starting point.

We encountered an issue where the shortest path through hippocampal grey matter to the anterior and lateral parts of the hippocampus would sometimes pass through the medial part of the uncus, rather than going along the inferior side of the hippocampus. To mitigate this issue, we applied the Fast Marching algorithm to individual slices along the pseudo-geodesic anterior-posterior gradient computed in the previous step (50 slices divided equally along the anterior-posterior gradient), and then normalized the distances to a range of 0-1000 within each slice. This normalization accounts for the fact that the hippocampus is wider in some areas (e.g. the distance will be greater when a slice passes through a digitation). Because the gradient was not perfectly aligned between slices, we then performed smoothing using five iterations of an averaging filter. This resulted in a continuous gradient along the proximal-distal axis of the hippocampus, that changes perpendicularly to the anterior-posterior gradient and in parallel to the borders of the hippocampal subfields (see Results section 3.4; Figure 5). This corresponds to step (v) in section 2.5.

## 2.10 Defining subfield borders

The anterior-posterior gradient and the proximal-distal gradient together make up a 2D coordinate system for indexing any column of hippocampal grey matter. Using this coordinate system we can define each subfield boundary with a relatively simple set of

rules. We made the assumption, based on Ding *et al.*'s recent histology work<sup>37</sup> and on the folding of hippocampal grey matter during development<sup>15</sup>, that all subfields would be present throughout the pseudo-geodesic anterior-posterior extent of the hippocampus. Thus, we must determine an appropriate proximal-distal distance to demark the borders of each subfield. The coordinate system being used already accounts for digitations and the curvature of hippocampal grey matter in the hippocampal head and tail, which are features that are missing from other manual segmentation protocols. As an initial proof of concept, we chose boundaries that would remain constant across the anterior-posterior extent of the hippocampus and across people. This was done by adjusting each boundary in two reference hippocampi until all borders in the computationally segmented hippocampi resembled their manually segmented counterparts. Note that the manual segmentation was performed primarily using Ding *et al.*'s recent histological study of the hippocampal head<sup>37</sup>, and this work was again consulting when choosing boundary distances for each subfield, as well as Duvernoy's monograph<sup>15</sup> to try and achieve the most accurate subfield borders for these two hippocampi. The subfield boundaries we chose can be expressed as a percentage of their pseudo-geodesic distance along the proximal-distal gradient: subiculum-CA1 at 34%; CA1-CA2 at 65%; CA2-CA3 at 72%; CA3-dentate gyrus at 85%. This corresponds to step (vi) in section 2.5, and this selection of border definitions was used in all segmentations.

Subfield labels were applied to hippocampal grey matter in the native MRI space by indexing all voxels in the proximal-distal gradient that fit each of the chosen border distances (corresponding to step (vii) in section 2.5). We reasoned that since the subfield boundaries generalized well between a highly digitated and a less digitated hippocampus, they would likely be appropriate for segmenting the remaining set of hippocampi. We applied these border distances to each of the remaining hippocampi and visually assessed whether the subfields were placed appropriately (again, based on Ding *et al.*<sup>37</sup> and Duvernoy's monograph<sup>15</sup>).

Based on previous work, we know that subfield borders vary somewhat across the anterior-posterior extent of the hippocampus<sup>49</sup>, and vary significant between individuals in relation with many factors (e.g. age, sex, stress, cognitive ability, hormonal

fluctuations, and the presence of diseases). Thus, ideally, the proximal-distal borders of each subfield should vary along the anterior-posterior gradient to best fit the true subfield locations, and should be further adjusted based on any additional available image features. Gross morphological features (e.g. most lateral edge of the hippocampus; presence of extra-hippocampal structures) are typically accounted for in other manual segmentation protocols, as they will determine landmarks to be used as border rules. However, to our knowledge, no intra-hippocampal features have been reported for informing subfield segmentation in *in-vivo* MRI (besides the hippocampal dark band). As outlined in Introduction section 1.7, we had predictions about voxel intensities in the native MR images based on the cytoarchitecture of the different subfields. We saw hints of this while performing the initial manual translation of Ding *et al.*'s work<sup>37</sup>, but since intensity differences could not be seen in many slices, they were not a reliable feature for guiding manual segmentation. Using our 2D coordinate system, we were able to sample clusters of voxels in the original MR image along the anterior-posterior and proximal-distal gradients of hippocampal grey matter. We could then map out the average intensities along the anterior-posterior and proximal-distal axes. Intensities are generally higher in the posterior medial-temporal lobe because of better MR signal quality, so we normalized the intensities along the anterior-posterior axis. Using this technique, intensity differences appeared in bands along the proximal-distal axis that initially appear to correspond to hippocampal subfield borders (see Results section 3.5; Figure 6). We then mapped these intensities to the surface of a 3D model of hippocampal grey matter to visualize these intensity bands in 3D, and to compare to a 3D model of segmented subfields. Because of time constraints we have not yet adopted this intensity sampling evidence for adjusting subfield borders, but that is a direction that we are actively pursuing.

## 2.11 Reliability measures

Some of the steps in this protocol require manual input from a tracer, and so the reliability of segmentation was assessed between two raters (JD and KF), and across multiple traces by the same rater. This was done using Dice Similarity Index (DSI), as in most other manual segmentation protocols. This is defined by the following equation:

$$DSI = 2a/(2a + b + c),$$

where  $a$  is the number of voxels in both segmentations, and  $b$  and  $c$  both represent the number of voxels that are unique to each segmentation. Perfect overlap would produce a value of 1, and lower overlaps range from 0 to 1. Inter-rater reliability was calculated for manually segmented labels from 6 hippocampi (3 left and 3 right) with varied numbers of digitations. Intra-rater reliability was also calculated for labels from 6 hippocampi, 3 of which were also used in inter-rater reliability. Only a subset of our MR data was segmented multiple times for reliability assessment in the interest of saving time. Errors in manual segmentation can produce major distortions on the unfolded hippocampal grey matter, so the unfolded grey matter tissue was examined by each rater to ensure their labelling followed the rules outlined in Appendix A. Where errors in the unfolding were obvious, segmentation was corrected before computing DSI. For easier comparison to other protocols, we chose to calculate DSI for grey matter and dark band combined as total hippocampal volume, as no other protocol segmented hippocampal grey matter as its own label.

The extra-hippocampal structures are not labelled in their entirety, but only where they border hippocampal grey matter. These labels are required only for the subsequent steps in subfield labelling. Thus, their reliability was not explicitly assessed, but the reliability of the subsequent unfolding and subfield labelling was assessed. We assessed the reliability of the overall subfield segmentation given by the manual tracing steps and the subsequent automated unfolding and labelling together. This was measured by inter- and intra-rater DSI, as in the other manually segmented structures. Note that the unfolding and border labelling performed here will depend on variability in manually labelled hippocampal grey matter and dark band but also variability in manually labelled extra-hippocampal structures which was not accounted for when we assessed reliability of other manually traced structures.

### 3 Results

Manually segmented reference hippocampi were traced and examined in detail. Results from the various steps of our semi-automated segmentation protocol were then examined.

#### 3.1 Manually segmented reference hippocampi

By directly lining up coronal MRI slices with Ding *et al.*'s histologically stained slices of the hippocampal head<sup>37</sup>, we were able to segment the entire head in detail in two hippocampi - one highly digitated and one with few digitations. Figure 2a shows a representative segmented slice from the hippocampal body, where the dark band is the only intra-hippocampal structure that is readily apparent. Given that the positioning of the subfields is highly consistent along the longitudinal axis of the hippocampal body, their morphology can be described with a relatively simple set of rules, as proposed in many previous subfield protocols (see Figure 2a). Arrows in Figure 2a indicate potential protocol rules: the dark band where it is visible (left arrow); the border of subiculum-CA1 is half-way along the width of the dentate gyrus (bottom arrow), and the CA1-CA2 border is a line directly above the most lateral part of the dark band (right arrow). In the hippocampal head, however, subfield borders are often parallel to the coronal plane. It is very difficult to predict where each subfield should lie just by looking at an individual coronal plane (e.g. Figure 2b). Furthermore, subfield positions change dramatically between slices in the hippocampal head. Similar issues are observed in the sagittal and axial planes.

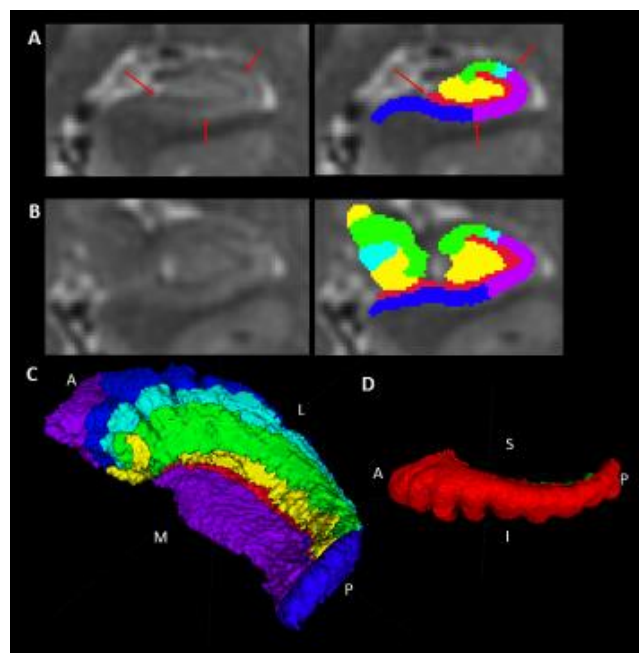


**Figure 3. Manual segmentation and translation of histological characterization of hippocampal subfield by Ding *et al.* <sup>37</sup>. Purple shows the subiculum, blue CA1, cyan CA2, green CA3, yellow dentate gyrus, and red shows hippocampal dark band. A) MRI slice from the hippocampal body (left) and the labelled subfields in that image (right). Arrows indicate potential protocol rules (see text). B) Same structures as A), but in the hippocampal head where the uncus can be seen on the medial side. C) 3D model of all subfields throughout the hippocampus. D) Example hippocampus not separated into subfields, but demonstrating the digitations in the hippocampal head continuing along the lateral and inferior side of the body.**

Ding *et al.* <sup>37</sup> suggest that these issue could be overcome by using the digitations in the hippocampal head as additional landmarks, and make an effort to describe subfield borders with respect to digitations for easier translation to MRI. However, we encountered several challenges that revealed limitations of this sort of landmark-based segmentation: 1) different hippocampi have different numbers of digitations, so additional rules must be used accordingly; 2) the digitations are primarily perpendicular to the borders of different subfields (i.e. proximal-distal) so subfields don't follow the folding and it can be unclear where exactly the proximal-distal edges of a digitation are as it recedes back into the rest of the hippocampus; 3) some hippocampi have 3-5

digitations as Ding *et al.* described, but others have more digitations that appear to continue all the way along the length of the hippocampal body on its lateral and inferior side (Figure 2d), so it is unclear which digitations should be used as any given landmark.

Examination of 3D finished segmentation models revealed some potentially useful regularities. Results for the highly digitated hippocampus are shown in Figure 6c and d, but were similar for the partial segmentation of a less digitated hippocampus as well. The borders of each subfield follow a smooth, continuous trajectory parallel to the curve of the uncus. In 3D modelling terms, we could consider each subfield to be a folded and curved ‘ribbon’ or ‘strip’ of some length and width running along the anterior-posterior extent of the hippocampus. Each subfield also has a relatively constant thickness, and bordered the hippocampal dark band on its internal side (except for the dentate gyrus, which is inside the dark band, and subiculum which extends medially past the dark band) and non-hippocampal structures on the external side. The hippocampal dark band thus might be considered a sort of ‘skeleton’ for the rest of the hippocampus, with hippocampal grey matter wrapping around it in all directions or ‘draped over’ it like a fabric that is fixed inside the dark band as in the dentate gyrus, and extending medially from it as in the subiculum. This hippocampal grey matter is continuous along the proximal-distal and anterior-posterior extent of the hippocampus. Each of these features is in correspondence with Duvernoy’s and Ding *et al.*’s descriptions of hippocampal anatomy<sup>15,37</sup>, and must necessarily be present due to the folding of the hippocampus during development, but hasn’t explicitly been leveraged in any subfield segmentation protocol that we know of.

## 3.2 Dark band dilation technique

We were able to guide segmentation of hippocampal grey matter by first tracing and then dilating a label for the hippocampal dark band. We expected this would be a reliable technique given that the dark band is the most obvious intra-hippocampal feature in our images (e.g. Figure 2a left). Examination of a 3D model of dark band label (Figure 2a right) reveals several features about hippocampal morphology: the dark band elucidates the curvature of the hippocampus along its longitudinal axis as well as the extent of folding in the proximal-distal axis. From the dark band label we can also clearly see the

number and locations of digitations in the hippocampal head and body, which is highly variable between subjects. The hippocampal dark band thus contains spatial information about the overall morphology of the hippocampus that is highly specific to each individual.

Following the user-guided dilation of the hippocampal dark band, we were able to quickly label most of the volume of hippocampal grey matter. Notable exceptions were in the vertical component of the uncus, the subiculum, and adjustments required along the medial border (Figure 3b,c). We estimate that it took 30 minutes to trace the dark band, and 1 to 2 additional hours to label all hippocampal grey matter for an experienced tracer. This is much faster than labelling all of hippocampal grey matter by hand, which, given the high resolution of our data, we estimate would take more than 4 hours for experienced tracers (without tracing of the dark band). Dark band segmentation, dilation, and manual adjustments are depicted only for a highly digitated hippocampus, but results were similar in all other hippocampi.

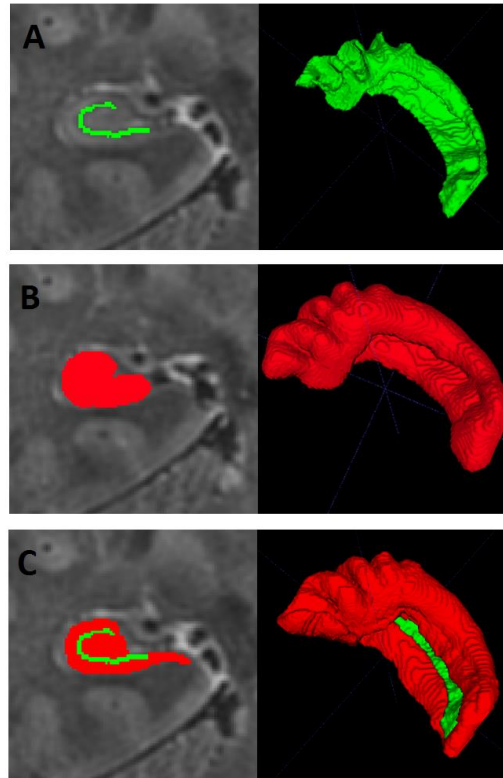


**Figure 4. Dilation and manual adjustments of dark band to generate hippocampal grey matter volume. A) Dark band trace on individual slice (left), and a 3D model of the dark band (right). B) Dark band is dilated until it reaches the external border of hippocampal grey matter on the inferior, lateral, and superior sides (left), producing a 3D model (right) containing most of hippocampal grey matter. C) Manual adjustments to remove grey matter label where it was incorrectly labelled and add grey matter label where it was missed.**

### 3.3 Hippocampal grey matter unfolding

Figures 4 and 5 show the results of unfolding hippocampal grey matter along the pseudo-geodesic anterior-posterior and proximal-distal gradients, respectively. These models were made by binning each of these gradients into segments, excluding the hippocampal dark band. In the anterior-posterior unfolding, we can see that each ‘slice’ or anterior-posterior bin shows the folding of hippocampal grey matter into the classic ‘C’ shape. In the hippocampal head, this folding becomes distorted due to the digitations, but nevertheless grey matter is composed of a single, continuous tissue wrapping around the

dark band. The most medial part of the hippocampal head, the vertical component of the uncus, takes on a slightly different shape as the folded ‘C’ shape flattens out. This description matches results reported in Ding *et al.*’s recent histological study<sup>37</sup>. Another interesting feature of the anterior-posterior gradient is that the proximal part of many slices is shifted more anterior to its distal part, which in turn is shifted more posteriorly. This is because on the inferior side of the uncus, the border with medial-temporal lobe cortex extends more anteriorly than most of the rest of the uncus.

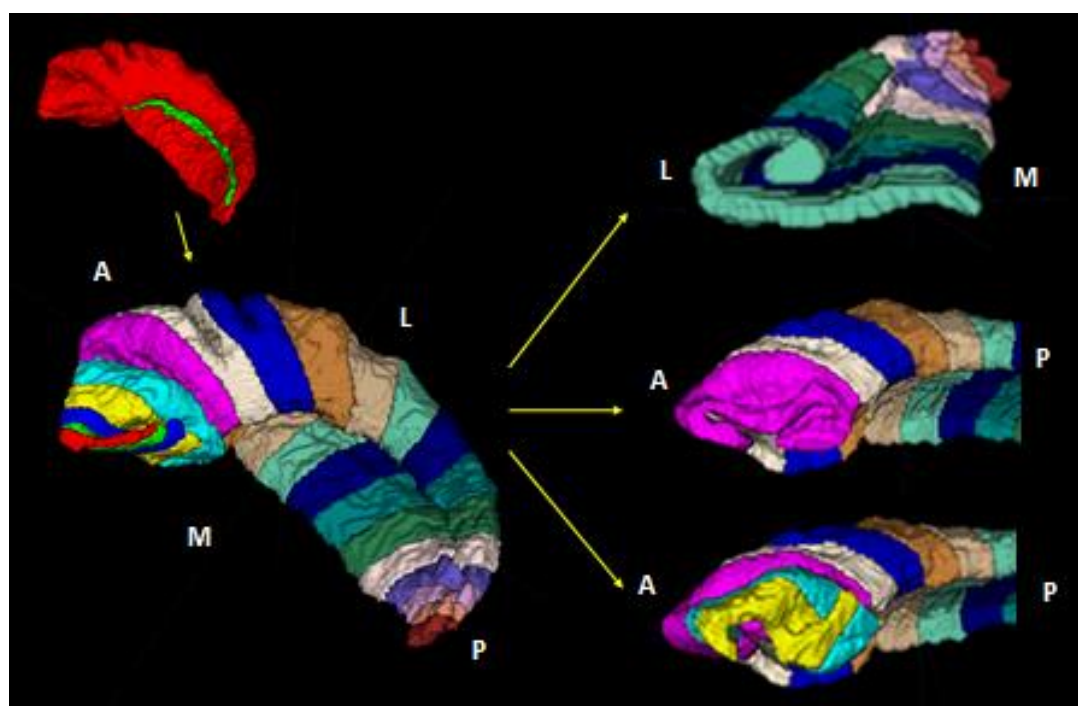


**Figure 5. Anterior-posterior unfolding of hippocampal grey matter using the Laplacian equation. The anterior-posterior extent of hippocampal grey matter (top left) is labelled with scalars, which are binned into slices (bottom left). Cross-sections along these bins reveal the classic hippocampal ‘C’ shape (right), except in the vertical component of the uncus (bottom right).**

Turning to the proximal-distal unfolding of hippocampal grey matter, we can see that borders between bins or ‘strips’ are more jagged. This is an artifact of the fact that unfolding was performed separately for each anterior-posterior slice, and so the proximal-distal gradients aren’t perfectly aligned. We found that performing the proximal-distal

unfolding on all hippocampal grey matter combined would produce other challenges: the shortest distance to some of the most lateral and anterior parts of the hippocampus would pass through posterior-superior parts of the uncus rather than the inferior side of the hippocampus, producing incorrect unfolding. Smoothing was applied to overcome this issue, but had to be limited because areas where the proximal-distal gradient was steep (i.e. thin parts of the hippocampus such as the tail or vertical component of the uncus) would otherwise become erroneously rescaled. That is, the most proximal and distal parts of the gradient would have their values reduced in proportion to the steepness of the gradient in that slice. One other issue is that the most distal bin of the proximal-distal gradient, corresponding to the most inner parts of the dentate gyrus, is sometimes discontinuous in the midsection of the vertical component. Unfolding is depicted only in a highly digitated hippocampus, but results were similar in all other hippocampi.

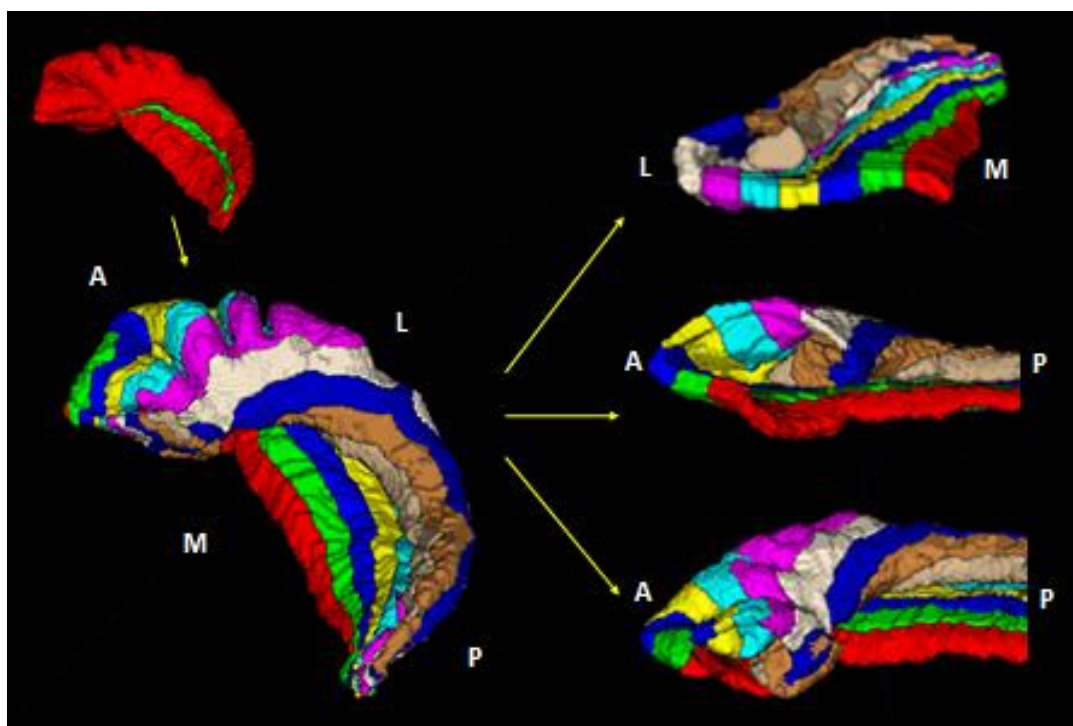


**Figure 6. Proximal-distal unfolding of hippocampal grey matter using the Fast Marching algorithm. The proximal-distal extent of hippocampal grey matter (top left) is labelled with scalars, which are binned into strips (bottom left). Slices along the previously described anterior-posterior extent show the labelling within the length of the classic hippocampal ‘C’ shape (right).**

### 3.4 Completed segmentation morphologies

We chose to apply constant proximal-distal borders along the unfolded anterior-posterior gradient for each subfield in all hippocampi. The constants were chosen based on the best possible matching of two hippocampi to their corresponding fully manual segmentations, corroborated by Ding *et al.*'s histology and Duvernoy's monograph<sup>15,37</sup>. We applied those borders to the unfolded hippocampal grey matter of all remaining hippocampi, and then carried the resulting labels back through the unfolding transformation. We modelled all subfields in their native space, which can be viewed in Figure 6.

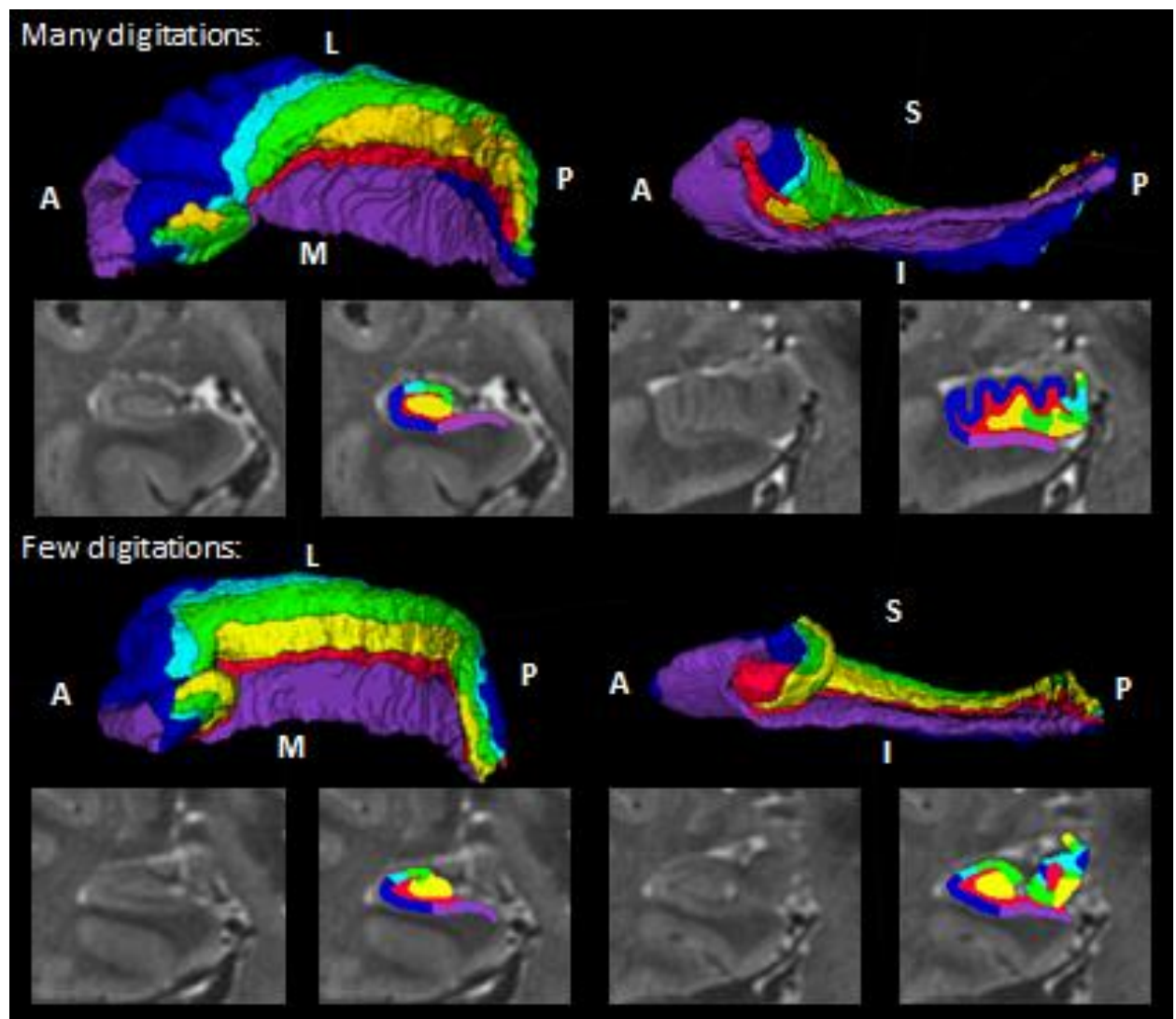


**Figure 7. Finished segmentation of two hippocampi: one with many digitations (top) and one with few digitations (bottom). Left models viewed from above and medial,**

**right models from medial and slightly below. Below the models are example coronal slices from the hippocampal body (two left images; with and without subfields imposed) and head (two right images).**

There are large morphological differences between the two hippocampi depicted in Figure 6. One hippocampus is highly digitated and with a very gentle curve of all subfields in the uncus (i.e. a gradual medial curve in the uncus), while the other hippocampus has only few digitations and has a much steeper curve in the uncus. Furthermore, the highly digitated hippocampus appears to show less proximal-distal folding towards their posterior and more in the anterior as compared to the less digitated hippocampus. Even with these gross differences, both hippocampi were very closely matched to their manually segmented counterparts (e.g. compare Figures 4 and 8) and to the Ding *et al.* recent histological study<sup>37</sup>. Seven out of eleven hippocampi that we segmented in the current study showed some extent of digitation within the hippocampal body (Figure 2d most prominent example). The remaining 4 more closely resembled the less digitated hippocampus. The morphologies of the hippocampi observed in our sample did not cluster into apparent categories based on their numbers of digitations as suggested by Ding *et al.*<sup>37</sup>, but rather spanned a range of morphologies. Mean subfield and total hippocampal grey matter volumes are shown in Table 1.

**Table 1. Mean volumes (mm<sup>3</sup>) of manually or user-guided segmented structures (dark band and hippocampal grey matter) and automatically segmented structures (subiculum - dentate gyrus) in left and right hippocampi.**

	Right		Left	
	Mean	SD	Mean	SD
Dark band	620.6	66.2	644.7	76.1
Grey matter	2538.0	176.0	2428.5	248.7
Subiculum	754.6	72.2	816.1	76.3

CA1	879.6	86.2	807.3	106.5
CA2	134.5	13.9	128.3	30.7
CA3	346.1	77.9	296.0	71.2
Dentate gyrus	423.4	38.1	380.9	78.8

### 3.5 Reliability of manually traced and automatically segmented structures

Reliability for manually segmented structures and user-guided or automatically segmented structures was calculated using DSI, as in other protocols for segmenting hippocampal subfields (e.g. <sup>28-31</sup>) (Table 2). For manually segmented structures, reliability was very high. The dark band is the most obvious intra-hippocampal image feature in our data (Figure 2a), and as such, we anticipated that its tracing reliability would be high despite the fact that thin structures typically produce lower DSI. Intra-rater reliability DSI was  $M=0.68$ ,  $SD=0.04$ , whereas inter-rater DSI was  $M=0.72$ ,  $SD=0.03$ . Intra-rater reliability DSI for resulting grey matter label was  $M=0.92$ ,  $SD=0.01$ , whereas inter-rater DSI was  $M=0.91$ ,  $SD=0.03$ .

DSI for the automatically segmented hippocampal subfields (which are divisions of hippocampal grey matter) were calculated to assess the effects of variability in manual traces on our unfolding and segmentation. These DSI scores will depend both on variability in grey matter and dark band traces, and the tracing of extra-hippocampal structures. In particular, the extent to which grey matter of the subiculum and vertical component of the uncus protrude from the rest of the hippocampus will produce a systematic shift in the proximal-distal gradient, changing all subfield borders. In spite of this, we saw moderate to good inter- and intra-rater reliability for all subfields.

Specifically, we saw only low to moderate DSI scores in our protocol for the smallest subfields CA2 and CA3 (0.34 to 0.61), good DSI in the dentate gyrus (0.65 to 0.70), and very good DSI in subiculum and CA1 (0.73 to 0.77).

**Table 2. Inter- and intra-rater reliability measures (Dice Similarity Index) for manually or user-guided segmented structures (dark band and total hippocampal volume) and automatically segmented structures (subiculum - dentate gyrus).**

	Intra-rater		Inter-rater	
	Mean	SD	Mean	SD
Dark band	0.68	0.04	0.72	0.03
Total hippocampus	0.92	0.01	0.91	0.03
Subiculum	0.76	0.04	0.73	0.05
CA1	0.77	0.02	0.73	0.04
CA2	0.46	0.05	0.34	0.09
CA3	0.61	0.02	0.50	0.07
Dentate gyrus	0.70	0.05	0.65	0.06

### 3.6 Intensity differences across subfields

To probe the usefulness of intensity differences for segmentation of hippocampal subfields, we sampled grey matter voxels in the native MR image according to proximal-distal and anterior-posterior gradient bins (100 evenly spaced bins in each dimension). Figure 7a shows a representative mapping of the resulting mean intensities. Areas corresponding roughly to subiculum appear dark, CA1 appears bright, CA2 and CA3 appear dark, and the dentate gyrus appears especially bright. The border between CA1 and CA2 closely matches the most lateral part of hippocampal grey matter, which is a very commonly used as a reliable border between these structures in other protocols in the hippocampal body <sup>27</sup> (though, notably, that rule doesn't hold true in the hippocampal

head or tail). It should be noted that some indices contained no corresponding voxels in the native MR image (e.g. if the geodesic distance along one axis was less than 100 voxels in the native image), so they appear dark in Figure 7a. We then mapped the intensity differences onto the surface of a 3D model of hippocampal grey matter (Figure 7b). A qualitative comparison between a 3D segmentation model and the grey matter model with intensities mapped onto it shows that the brighter areas typically correspond to CA1 and the dentate gyrus, whereas darker areas typically correspond to CA2, CA3, and the subiculum. Note that the intensity differences didn't always follow such clean anterior-posterior bands for all hippocampi, but we chose to illustrate this example to most clearly show the general trend. Although the results reviewed are only preliminary, and do not include a formal assessment of the value of intensity differences as a marker for subfield segmentations, they reveal some promise for formal implementation in future work.

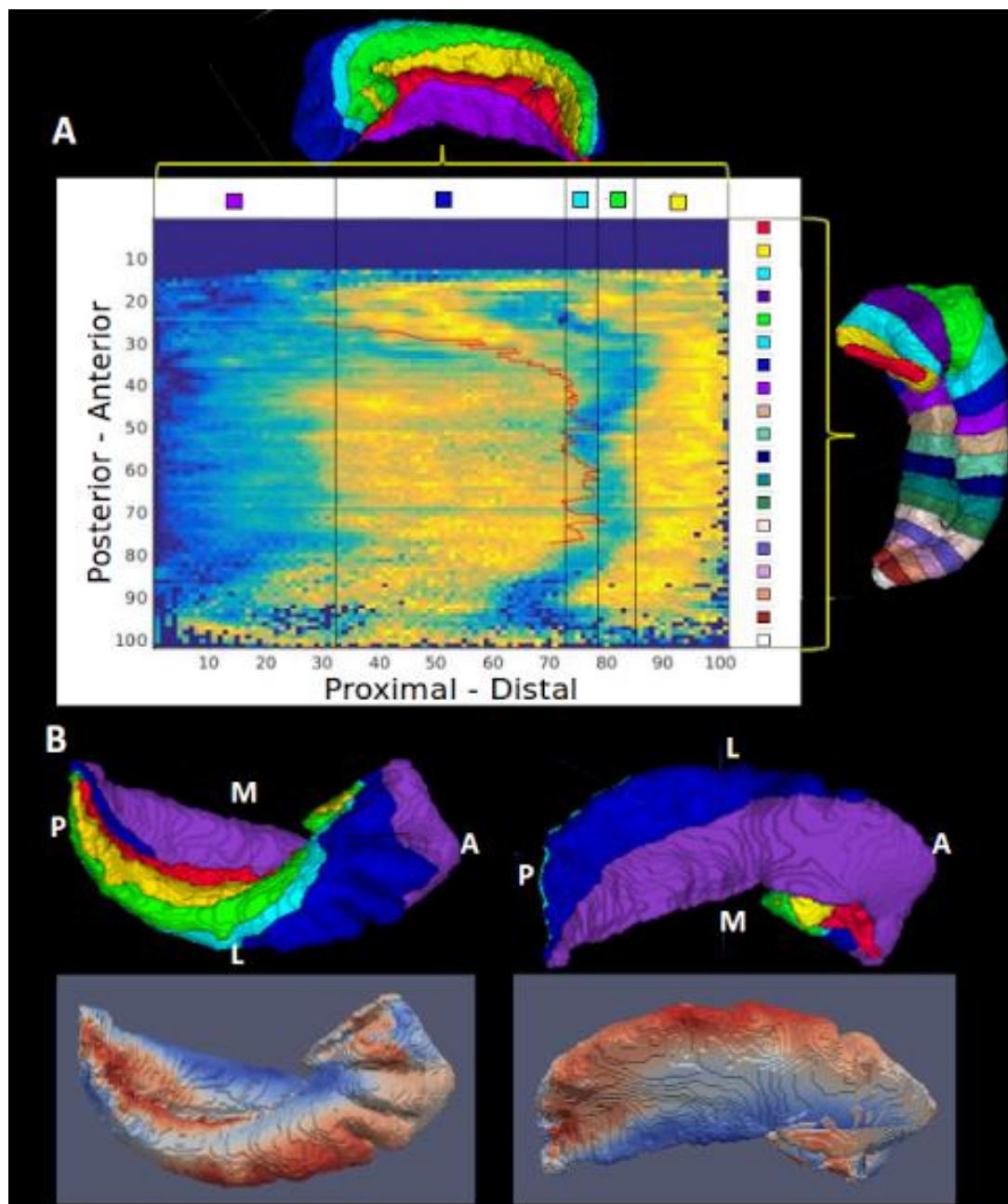


**Figure 8.** Native MRI voxel intensities across anterior-posterior and proximal-distal gradients. Warm colours indicate high intensities. A) 2D map of normalized voxel intensities. Vertical lines show the subfield boundaries, as mapped onto the 3D model above. The red line indicates the most lateral edge of the hippocampus. B) Subfield models (top) and grey matter model with corresponding voxel intensities mapped onto its surface (bottom) shown from above (left) and below (right).

## 4 Discussion

Manual segmentation with high anatomical detail presents many challenges for the generation of a simple and reliable protocol for tracing hippocampal subfields.

Considerations of regularities in hippocampal structure and ontogeny offer ways in which computational tools can be applied for detecting, indexing, and segmenting hippocampal tissue. In the current study we pursued an approach that took advantage of such considerations, using intra-hippocampal features that have not been considered in prior work on hippocampal segmentation. The resulting protocol produced moderate to good reliability, and shows promise for formal implementation in future research.

### 4.1 Limitations elucidated by manually segmented reference hippocampi

We performed fully manual segmentations based on the recent histological study by Ding *et al.*<sup>37</sup>, but this presented many challenges for creating a reliable protocol for subfield segmentation. We found that the number of rules required to achieve detailed hippocampal subfield segmentations in the complex structure of the hippocampal head would be unfeasibly high. That is, the general shape of each subfield changes dramatically between slices through the hippocampal head in all orientations, meaning that there is little consistency in the geometric rules that can be used to describe subfield locations as in the hippocampal body. There are two reasons for this inconsistency between slices: the curvature of the uncus and the digitations (folding) of hippocampal grey matter. The uncus curves medially, posteriorly, and then superiorly, so in principle a cross-section of the uncus could be achieved using the coronal, sagittal, coronal, and then axial planes for viewing. However, this also proved challenging due to the digitations in the hippocampal head that would obscure the classic ‘C’ shape seen in cross sections of the hippocampal body.

We attempted to apply Ding *et al.*’s histologically-based emphasis on the locations of digitations in the hippocampal head, but again encountered problems: (i) different hippocampi have different numbers of digitations, so additional rules must be used

accordingly; (ii) the digitations run primarily perpendicular to the borders of different subfields and it can be unclear where exactly the proximal-distal edges of a digitation are as it recedes into the rest of the hippocampus; (iii) some hippocampi have 3-5 digitations as Ding *et al.* describe, but others have more digitations that appear to continue all the way along the length of the hippocampal body on its lateral and inferior side (Figure 2d), so it is unclear which digitations should be used as a given landmark. Thus, we turned to computational tools to help guide and constrain segmentation in hopes of coming up with a reliable protocol while respecting the high level of anatomical detail available.

## 4.2 Value and limitations of hippocampal grey matter unfolding

All of the hippocampal subfields originate from a single, folded piece of grey matter tissue. During development, different parts of this tissue become specialized and take on the cytoarchitecture that defines the hippocampal subfields, but their spatial relationship as being located on adjacent strips of a continuous tissue is preserved. This tissue folds upon itself making a stereotyped ‘C’ shape in cross sections of the hippocampus, and also curls medially in the head and tail of the hippocampus, and posteriorly and upwards in the hippocampal head. Broadly speaking, our approach to subfield segmentation was to unfold this hippocampal grey matter tissue along its anterior-posterior and proximal-distal axes.

Unfolding hippocampal grey matter along its anterior-posterior extent resulted in a gradient that followed the curvature of the hippocampal head and tail. In these slices, we were able to recover the stereotyped hippocampal ‘C’ shape. In the vertical component of the uncus this ‘C’ shape became flattened out, but nevertheless closely matched Ding *et al.*’s descriptions<sup>37</sup>. The anterior-posterior unfolding also produced an unforeseen feature: the proximal part of many slices is shifted more anterior to its distal part (see Figure 4). It remains unclear at present whether this has to do with the way hippocampal tissue folds during its development, and whether it reflects true connectivity between hippocampal subfields, but it is interesting to note for future investigation. If the connectivity between subfields in cross sectional slices is not misaligned from anterior to posterior, as in our anterior-posterior slicing, then it may be that in the anterior of the

hippocampus, the more distal regions of the hippocampus (e.g. dentate gyrus) project to relatively thinner areas in proximal subfields (e.g. subiculum). This might explain why some studies have found the subiculum to be relatively larger in the more posterior hippocampus<sup>49</sup>, and indeed may have to do with functional specialization along the long axis of the hippocampus<sup>49,50</sup>.

The proximal-distal axis of the hippocampus is parallel to the borders of the subfield, and so subfields can be indexed according to their distance along this gradient. Thus this gradient is most of interest for drawing subfield borders. We found that using the anterior-posterior gradient to constrain proximal-distal unfolding (by running proximal-distal unfolding in separate anterior-posterior bins) produced optimal results. However, this did introduce the problem of imperfect alignment between anterior-posterior slices. As presented in Methods section 2.10, this issue is partially resolved through smoothing, but minor distortions in some areas of the proximal-distal gradient remain. This reflects a limitation of the methodology used here, and may have a putative effect on subfield reliability measures that we obtained.

As mentioned in the results section, proximal-distal unfolding produced an error in some hippocampi such that the most distal regions would not be continuously connected in the vertical component of the uncus (Results section 3.3). In reality we know that the most distal subfield, the dentate gyrus, is continuous and should wrap medially around the more proximal CA3 before extending upwards to take its place in the most distal part of the vertical component of the uncus. This is another limitation of our proximal-distal unfolding technique, and may have to be resolved in future work by introducing additional rules to make the most distal label continuous. However, the proximal-distal unfolding does naturally place the most distal labels correctly in the inferior and superior segments of the vertical component of the uncus, which can be challenging to do even in manual tracing given the smallness of the subfields in this area and lack of intra-hippocampal image features.

It is worth noting that similar proximal-distal unfolding has been performed in medial-temporal lobe cortex and hippocampal subfields in prior work. Several studies reported

by Bookheimer and colleagues have implemented a technique to segment the grey matter of the medial temporal lobe cortex and hippocampal subfields along the dark band, and then computationally flatten out this tissue (see <sup>51,52</sup> and also in 7T MRI <sup>53</sup>). However, this technique makes use of a different set of flattening algorithms, and does not fully account for the curvature in the uncus. Furthermore, the flattening technique used by Bookheimer and colleagues does not serve as a coordinate system for segmenting hippocampal subfields. Instead, borders are determined in the native space of the hippocampus by anatomical landmarks, geometric rules, and reference to Duvernoy's monograph <sup>15</sup>, before then being carried forward through the unfolding for the purpose of visualizing data. Nevertheless, the fact that the hippocampus and surrounding cortex could be visualized in this flattened plane nicely demonstrates their preserved, single tissue structure.

### 4.3 Consideration of completed subfield morphologies

To index the borders between the different hippocampal subfields we applied constant proximal-distal distances for each subfield along the entire anterior-posterior extent of the hippocampus, for all hippocampi. This was informed by our reference manual segmentations, but also reaffirmed with Ding *et al.*'s histology study and Duvernoy's monograph <sup>15,37</sup>. Given that our proximal-distal gradient also follows the curvature and folding anterior-posterior gradient, each subfield correctly follows these digitations and curvature, and has its natural termini correctly in the vertical component of the uncus. This is a critical feature missing from all other current segmentation protocols <sup>27</sup>. Another unique feature of our segmentation approach that is missing in other protocols is that it captures the fact that the subiculum wraps around the superior side of the anterior hippocampus. In our protocol, this arises from the morphology of our proximal-distal gradient, which shifts distally in the anterior of the hippocampus as the border between subiculum and medial-temporal lobe cortex shifts superiorly and medially.

Note that the distances we use for indexing subfield borders represent a somewhat rough first attempt at using this unfolding technique, and there is likely room for improvement by leveraging additional intra-hippocampal MR image features (see section 4.5).

However, based on comparison to our reference models and on the account of Ding *et al.*

and Duvernoy<sup>15,37</sup>, these border distances lead to improved segmentation accuracy even in hippocampi with different gross morphological features (Figure 6; Results section 3.4). This finding suggests that the differentiation of hippocampal subfields during development is relatively constant across ‘unfolded’ hippocampal grey matter, and it is rather the folding of this tissue that leads to the largest inter-individual differences in subfield locations.

Although overall morphology was different from other studies<sup>27</sup>, reflecting the incorporation of recent advances in anatomical knowledge about the hippocampal head, the volumes of each subfield reported in this study are within the range of those found by other studies.

#### 4.4 Reliability of manually traced and automatically segmented structures

Tracing the dark band and hippocampal grey matter (following dilation of dark band and manual adjustments) was expected to be reliable given that the dark band is easily visible under our imaging protocol. Manual traces showed very good inter- and intra-rater DSI, indicating good reliability (Table 1). Because not all hippocampal subfield tracing protocols provide equivalent labels to ours, we compared our inter- and intra-rater reliabilities to three prominent protocols to best cover a range of different image acquisition techniques and label choices: one at 3T, one at 7T, and one in *ex-vivo* tissue at 9.4T<sup>(28,31,30)</sup>, respectively). Because not all structures are given equivalent labels, we made comparisons only where appropriate labels are available. Note that DSI tends to be lower at higher resolutions because of the thin (i.e. high surface area to volume ratio) nature of hippocampal tissue and variability at the borders. For the dark band, our DSI scores were the same as Winterburn *et al.*’s 3T study (ours ~0.01 lower) and higher than manual and automatic labelling from Yushkevich *et al.*’s 9.4T study (ours ~0.13 higher). For total hippocampal volume (i.e. hippocampal grey matter and dark band), our scores were the same as Winterburn *et al.* (ours <0.01 higher) and higher than Wisse *et al.*’s 7T study (ours ~0.07 higher). Furthermore, our technique reduced the amount of time required to perform manual labelling of the entire hippocampus at such high resolution from more than four hours to less than two hours per hippocampus, and provides the dark

band label (which would not yet have been segmented in other protocols for whole hippocampal tracing). Since most manual segmentation protocols include the initial labelling of hippocampal grey matter, we recommend this technique for anybody attempting to segment sufficiently high resolution MRI data, whether implementing the subsequent steps of our protocol or not. Total hippocampal and dark band volumes were within the range reported by these studies.

The unfolding and segmentation into subfields of hippocampal grey matter is performed completely computationally and it will always produce the same results for a given input. We thus sought to determine whether differences in manual labelling would carry forward into differences in the computational unfolding and subfield labelling. Manual tracing of dark band and hippocampal grey matter were found to be highly reliable, but the smaller subfields of the hippocampus may be particularly vulnerable to any variability, which has been noted in other protocols (e.g. <sup>28-31</sup>). In addition, variability in extra-hippocampal structure labelling will contribute to variability in the unfolding and subfield segmentation, but it would not be appropriate to calculate DSI for these structures alone because our protocol traces them only where they border the hippocampus rather than their full volume, and the extent that a tracer extends the label past the border of the hippocampus is up to them and doesn't affect subsequent unfolding and subfield labelling. However, the area where manual tracing of these structures borders hippocampal grey matter will affect subsequent unfolding and subfield labelling, so they do likely contribute some variability to the finished subfield border locations.

We compare our segmentation results to other prominent segmentation protocols: again, one at 3T, one at 7T, and one in *ex-vivo* tissue at 9.4T (<sup>28,31,30</sup>, respectively). The subiculum, CA1, and dentate gyrus DSI scores were slightly below each of these studies (ours ~0.10 lower). CA2 and CA3 were grouped together by Winterburn *et al.* (3T) and by Yushkevich *et al.*, (9.4T) but in comparison to Wisse *et al.* (7T) our results were quite a bit lower (ours ~0.35 lower in CA2 and ~0.15 lower in CA3). We have identified several possible sources for this reduced reliability: the fact that DSI was lower for the smaller subfields likely reflects a compounding of variability in the manual segmentation steps. For example, the length of the medial extension of the subiculum will cause all

other borders to shift slightly, since they are rigidly defined based on distance from the medial edge of subiculum. Smaller subfields will be more affected because that displacement will make up a greater proportion of that subfield volume.

In addition to compounding of variability in dark band and grey matter labels, the extra-hippocampal structures which determine the computational unfolding of hippocampal grey matter may have had an impact on the subsequent border labelling and reliability. For example, locations of extra-hippocampal structure labels may have affected the locations of the minor distortions in the proximal-distal gradient caused by imperfect alignment between anterior-posterior slices, leading to small distortions in subfield borders. These distortions were most severe in the middle of the proximal-distal gradient, near the borders of CA2. This issue presents a significant limitation in our protocol. However, there may be room for improvement by modifying the ways in which the subfield boundaries are determined. That is, rather than using a rigidly defined distance from the medial edge of subiculum, borders could be adjusted more flexibly based on gross morphology of hippocampal grey matter, or other participant-specific image features. This sort of flexibility could compensate to some extent for variability in manual tracing and for small distortions in the proximal-distal gradient, therefore reducing the variability in finished subfield volumes and improving DSI scores.

## 4.5 Future directions for further protocol improvement

As shown in Figure 7, we found preliminary support for our hypotheses about subfield-specific intensity cues in the native MR image. We hypothesized that subiculum, CA2 and CA3 would appear relatively dark, while CA1 and the dentate gyrus would appear relatively more intense. This notion is supported by the fact that we observed intensity differences in native MR voxels indexed by the anterior-posterior and proximal-distal gradients. In most hippocampi clear bands of brighter and darker intensities can be seen that closely correspond to our estimated subfield borders. Following this finding, we have become very interested in these intensity differences as a possible tool for improving both the reliability and accuracy of subfield labelling.

As discussed above, variation in manual traces can lead to differences in subfield border locations. However, if we can anchor certain indices in our unfolding to features in the native MR image then we may be able to compensate for some of this variability. One way which we considered doing this is by anchoring the proximal-distal gradient to some gross morphological features, such as the most lateral edge of the hippocampus (which is often used to demark the boundary between CA1 and CA2). This would lessen the impact of variability in manually traced structures, improving reliability, but there is still no definite reason why the CA1/CA2 border must always follow the lateral edge of the hippocampus. Inter-individual differences may cause this border to be shifted in some hippocampi, and in our sample we even observed shifts in this border along the anterior-posterior extent of some hippocampi. If we instead use the native MR intensities to inform our definition of this boundary then the border can be allowed to shift based on inter-individual differences in MR images, improving the accuracy and generalizability of our protocol (particularly for individuals with diseases that might impact subfield size and locations). Because of time constraints, we have not yet developed a technique for determining these intensity-informed border definitions. This work will require tools that can implement prior expectations for where the borders should be, can implement constraints about border locations based on structural evidence (e.g. each subfield should terminate in the vertical component of the uncus and the tail of the hippocampus), and can flexibly fit intensity data. This work is currently in progress.

Intensity cues could potentially be a more valid way to determine subfield locations, but to date no protocol that we know of has explicitly leveraged these cues within hippocampal grey matter. It is not yet entirely clear what anatomical structures are driving these differences, and further investigation will have to be performed to determine their reliability and validity with respect to the true, histologically defined subfield locations. It is possible that intensity differences are primarily driven by subfield-specific vasculature, as described in Duvernoy's work <sup>15</sup>, which might explain why this feature has not been consistently observed in *ex-vivo* imaging with very high resolution and signal-to-noise, where we might expect the most obvious effects. We aim to investigate *ex-vivo* tissue using the same techniques to determine whether this is the case in a follow-up study. Another possibility is that the intensity differences are due to

partial-voluming with extra-hippocampal structures such as CSF or the white matter of the alveus. The alveus encircles all of the CA fields, and the subiculum is bordered on its inferior side by white matter of the rest of the medial-temporal lobe, so it is unlikely that this would lead to subfield-specific differences in intensities. Pockets of CSF, or cysts, can be seen throughout the hippocampus, but they typically appear sparsely scattered around grey matter and so would likely produce localized changes in intensity rather than consistent bands along the anterior-posterior gradient. Another possibility is that partial voluming interacts with the thickness of grey matter, such that thinner subfields are more affected than thicker ones. This is possible, particularly since CA3 is often thinner than the other subfields (described in Appendix A). However, if this were the case then that is still a valid cue for deriving subfield locations in healthy participants, since the thickness of hippocampal grey matter is also subfield-specific. Furthermore, we tried sampling data from only the middle 50% of the thickness of hippocampal grey matter and saw no gross differences in intensity patterns (data not shown), suggesting that intensity differences were not driven by partial voluming. Finally, the intensity differences could be driven by differences in myelin content, reflecting the cytoarchitecture that defines each subfield. In particular, the high number of recurrent collaterals in CA3 and the perforant path which passes through the subiculum might drive these effects.

With all of these considerations, it is most likely both the cytoarchitecture and the vasculature that together drive the intensity differences seen along the anterior-posterior and proximal-distal gradients of hippocampal grey matter in our data. Both of these possibilities represent valid cues for localizing subfields. Comparison between *in-vivo* imaging and segmentation and *ex-vivo* imaging and histology from the same participants' hippocampi is needed to validate this claim, which we aim to do in a follow-up study. A promising direction for future research involves the use data from patients with medial-temporal lobe epilepsy who receive *in-vivo* MR imaging and who subsequently have their afflicted anterior medial-temporal lobe resected as part of their clinical treatment. The resected tissue can be scanned with great resolution and then sectioned and histologically stained to determine the true locations of each subfield. This can be used to validate whether intensity differences and subfield location measured *in-vivo* correspond to this *ex-vivo* ground truth.

Another future direction for this protocol is reducing the amount of manual input required. Not only is this time consuming and requires expertise, but manual tracing also introduces variability that can be problematic when propagated forward into automated unfolding and subfield labelling. Specifically, the hippocampal dark band, grey matter, and extra-hippocampal structures should be automatically labelled such that they comply with the requirements for subsequent unfolding and labelling steps. The extra-hippocampal structures we used are often labelled by other automatic segmentation tools, such as FSL's FIRST<sup>54</sup> or Freesurfer's Subcortical and cortical segmentation<sup>55</sup>. The extra-hippocampal structures may not perfectly align with our highly detailed segmentation of the hippocampus, but their closest corresponding points on our segmentation could be a good way to determine the borders of hippocampal grey matter that our protocol requires. We are also exploring possible approaches to the problem of detecting and labelling the hippocampal dark band and surrounding hippocampal grey matter. .

## 4.6 Future applications

As mentioned in the Introduction section, many diseases are thought to affect some hippocampal subfields more than others. Better imaging and segmentation of the hippocampal subfields is anticipated to improve the quality of research on these topics, and eventually may be usable as a biomarker for disease in a clinical context. One prominent example of the utility of the tools developed in this study is in medial temporal lobe epilepsy, which has been shown to cause sclerosis and other abnormalities in some hippocampal subfields more than others<sup>56,57</sup>. Highly sensitive tools for imaging and detecting hippocampal subfields can be useful for two reasons. First, they allow for detection of abnormalities in otherwise MRI negative cases (as in<sup>58</sup>). Second, they allow for anatomically-guided subtyping of epilepsy to better predict clinical outcomes (as in<sup>59</sup>) *in-vivo*, before tissue resection. Most studies to date have focused on either the presence or absence of sclerotic tissue, overall volume, or morphology. However, our indexing system may reveal systematic pattern differences in intensity between healthy participants and epilepsy patients that may otherwise go unnoticed. Furthermore, examining the volume of individual hippocampal substructures could be a more sensitive

way of detecting abnormalities in cases that affect only some subfields and not others. Also, notably, it is typically the anterior hippocampus that is surgically resected and clinically effective in treatment of very severe epilepsies. Our particular attention to the complex structure of the hippocampal head may make our protocol well suited to examining abnormalities in this region. We are interested in pursuing this question in future research.

Another research area in need of improvement is the definition of hippocampal regions of interest (ROIs) for functional imaging. As discussed in the Introduction section, different subfields are associated with different computations, and the function of the hippocampus is thought to vary across its anterior-posterior extent<sup>49</sup>. Many questions remain as to how the hippocampal head differs in function from the body of the hippocampus. It could be that the subfields of the hippocampal head perform similar computations as in the hippocampal body but on different types of input information, given their different connectivity with extra-hippocampal structures (see<sup>38</sup>). Some subfields have a modified cytoarchitecture in the uncus, a feature that is particularly prominent in primates<sup>15</sup>, and so the computations they perform may differ from that of the corresponding subfields in the hippocampal body. Our protocol could lead to improvements in this research by improving the definitions of the subfields, and also the unfolding of hippocampal grey matter creates an easier way to visualize and index the continuous tissue of the hippocampus. Some researchers have discussed whether the hippocampus operates in discrete functional units along its anterior-posterior extent (e.g.<sup>60,61</sup>), but this has previously been challenging to test given the complex folding and curvature in much of the hippocampus. Our anterior-posterior unfolding may be an effective way to index these units. Finally, interesting proximal-distal differences within hippocampal subfields have been reported in the past<sup>62-65</sup>. With functional heterogeneity even within the hippocampal subfields, a greater degree of spatial specificity may be required to fully understand the function of hippocampal subfields and their relation to cytoarchitecture. Our proximal-distal unfolding may be a valuable tool for indexing these regions with high consistency despite inter-individual differences, particularly if the differences in voxel intensities across the proximal-distal gradient of hippocampal grey matter can be related to underlying cytoarchitecture or vasculature.

As mentioned above, some automated techniques already exist for performing hippocampal segmentation based on the use of atlases - the most advanced approach likely being ASHS<sup>32,36</sup>. However, these techniques are limited by the quality of the atlases on which they base subsequent segmentations. With this concern in mind, we aim to make our entire atlas of hippocampal traces from 12 participants publically available for further development of automated segmentation tools. We hope that this atlas will be used by other researchers to improve anatomical accuracy and detail when performing hippocampal subfield segmentation, leading to better quality research in the future.

## 4.7 Conclusion

We have developed a protocol for segmenting hippocampal subfields that respect the complex structure of the hippocampal head according to hippocampal ontogeny and recent structural evidence. This segmentation involves computational detection and unfolding of hippocampal grey matter, which provides a novel and potentially useful way of indexing subregions of the hippocampus while producing reliable subfield segmentation more quickly and easily than fully manual approaches. Results presented here suggest that this protocol offers sufficient precision and flexibility to accommodate inter-individual differences in morphology and produces segmentations that have improved accuracy and detail compared to other prominent protocols, with similar inter-rater reliability. Further anatomical validity promises to be achieved in the future by linking MRI features, specifically differences in image intensities, more systematically to distinct tissue properties.

## References

1. Rodríguez, F. *et al.* Spatial memory and hippocampal pallium through vertebrate evolution: insights from reptiles and teleost fish. *Brain Res. Bull.* 57, 499–503 (2002).
2. Mizunami, M., Makoto, M., Weibrecht, J. M. & Strausfeld, N. J. Mushroom bodies of the cockroach: Their participation in place memory. *J. Comp. Neurol.* 402, 520–537 (1998).
3. Malenka, R. C. & Bear, M. F. LTP and LTD: an embarrassment of riches. *Neuron* 44, 5–21 (2004).
4. Small, S. A., Schobel, S. A., Buxton, R. B., Witter, M. P., & Barnes, C. A. A pathophysiological framework of hippocampal dysfunction in ageing and disease. *Nature Reviews Neuroscience*, 12(10), 585–601 (2011).
5. Bergmann, O., Spalding, K. L. & Frisén, J. Adult Neurogenesis in Humans. *Cold Spring Harb. Perspect. Biol.* 7, a018994 (2015).
6. O'Keefe, J. & Dostrovsky, J. The hippocampus as a spatial map. Preliminary evidence from unit activity in the freely-moving rat. *Brain Res.* 34, 171–175 (1971).
7. Sherry, D. F. & MacDougall-Shackleton, S. A. Seasonal change in the avian hippocampus. *Front. Neuroendocrinol.* 37, 158–167 (2015).
8. Menzel, R. Searching for the Memory Trace in a Mini-Brain, the Honeybee. *Learn. Mem.* 8, 53–62 (2001).
9. Eichenbaum, H. & Howard, E. What H.M. Taught Us. *J. Cogn. Neurosci.* 25, 14–21 (2013).
10. Templer, V. L. & Hampton, R. R. Episodic memory in nonhuman animals. *Curr. Biol.* 23, R801–6 (2013).
11. Lee, A. C. H., Lok-Kin, Y. & Barense, M. D. The hippocampus and visual perception. *Front. Hum. Neurosci.* 6, (2012).
12. Cameron, H. A. & Glover, L. R. Adult neurogenesis: beyond learning and memory. *Annu. Rev. Psychol.* 66, 53–81 (2015).
13. Schacter, D. L. & Addis, D. R. The cognitive neuroscience of constructive memory: remembering the past and imagining the future. *Philos. Trans. R. Soc. Lond. B Biol. Sci.* 362, 773–786 (2007).
14. Winocur, G., Gordon, W. & Morris, M. Memory Transformation and Systems Consolidation. *J. Int. Neuropsychol. Soc.* 17, 766–780 (2011).
15. Duvernoy, H.M. *The human hippocampus*, Third edition, Springer-Verlag Berlin Heidelberg 2005 (232 pages).

16. Stylised diagram of the hippocampus. Wikimedia Commons: Hippocampus\_(anatomy). [https://commons.wikimedia.org/wiki/Category:Hippocampus\\_\(anatomy\)?uselang=en-gb#/media/File:Hippocampus\\_\(brain\).jpg](https://commons.wikimedia.org/wiki/Category:Hippocampus_(anatomy)?uselang=en-gb#/media/File:Hippocampus_(brain).jpg). Original image donated by Frank Gaillard Designs. First uploaded to the English Wikipedia as Hippocampus\_(brain).jpg. Modifications include cropping and inclusion of arrows denoting anatomical connectivity. This image is made available for use under the GNU Free Documentation License v1.3 (<https://www.gnu.org/licenses/fdl-1.3.html>).
17. Hunsaker, M. R., & Kesner, R. P. The operation of pattern separation and pattern completion processes associated with different attributes or domains of memory. *Neuroscience & Biobehavioral Reviews*, 37(1), 36-58 (2013).
18. Marr, D. Simple memory: a theory for archicortex. *Philos. Trans. R. Soc. Lond. B Biol. Sci.* 262, 23–81 (1971).
19. Deuker, L., Doeller, C. F., Fell, J. & Axmacher, N. Human neuroimaging studies on the hippocampal CA3 region - integrating evidence for pattern separation and completion. *Front. Cell. Neurosci.* 8, 64 (2014).
20. Knierim, J. J. & Neunuebel, J. P. Tracking the flow of hippocampal computation: Pattern separation, pattern completion, and attractor dynamics. *Neurobiol. Learn. Mem.* 129, 38–49 (2016).
21. Neher, T., Torsten, N., Sen, C. & Laurenz, W. Memory Storage Fidelity in the Hippocampal Circuit: The Role of Subregions and Input Statistics. *PLoS Comput. Biol.* 11, e1004250 (2015).
22. Liu, K. Y., Gould, R. L., Coulson, M. C., Ward, E. V. & Howard, R. J. Tests of pattern separation and pattern completion in humans-A systematic review. *Hippocampus* 26, 705–717 (2016).
23. Knierim, J. J. & Zhang, K. Attractor dynamics of spatially correlated neural activity in the limbic system. *Annu. Rev. Neurosci.* 35, 267–285 (2012).
24. Javanbakht, A. A neural network model for schemas based on pattern completion. *J. Am. Acad. Psychoanal. Dyn. Psychiatry* 39, 243–261 (2011).
25. Kyle, C. T., Stokes, J. D., Lieberman, J. S., Hassan, A. S. & Ekstrom, A. D. Successful retrieval of competing spatial environments in humans involves hippocampal pattern separation mechanisms. *Elife* 4, (2015).
26. Hindy, N. C., Ng, F. Y. & Turk-Browne, N. B. Linking pattern completion in the hippocampus to predictive coding in visual cortex. *Nat. Neurosci.* 19, 665–667 (2016).
27. Yushkevich, P. A. *et al.* Quantitative comparison of 21 protocols for labeling hippocampal subfields and parahippocampal subregions in in vivo MRI: towards a harmonized segmentation protocol. *Neuroimage* 111, 526–541 (2015).

28. Winterburn, J. L. *et al.* A novel in vivo atlas of human hippocampal subfields using high-resolution 3T magnetic resonance imaging. *Neuroimage* 74, 254–265 (2013).
29. Adler, D. H. *et al.* Histology-derived volumetric annotation of the human hippocampal subfields in postmortem MRI. *Neuroimage* 84, 505–523 (2014).
30. Yushkevich, P. A. *et al.* A high-resolution computational atlas of the human hippocampus from postmortem magnetic resonance imaging at 9.4 T. *Neuroimage* 44, 385–398 (2009).
31. Wisse, L. E. M. *et al.* Subfields of the hippocampal formation at 7T MRI: In vivo volumetric assessment. *Neuroimage* 61, 1043–1049 (2012).
32. Wisse, L. E. M. *et al.* Automated Hippocampal Subfield Segmentation at 7T MRI. *AJNR Am. J. Neuroradiol.* (2016). doi:10.3174/ajnr.A4659
33. Yushkevich, P. A. *et al.* Shape-based alignment of hippocampal subfields: evaluation in postmortem MRI. *Med. Image Comput. Comput. Assist. Interv.* 11, 510–517 (2008).
34. Van Leemput, K. *et al.* Model-based segmentation of hippocampal subfields in ultra-high resolution in vivo MRI. *Med. Image Comput. Comput. Assist. Interv.* 11, 235–243 (2008).
35. Wisse, L. E. M., Biessels, G. J. & Geerlings, M. I. A Critical Appraisal of the Hippocampal Subfield Segmentation Package in FreeSurfer. *Front. Aging Neurosci.* 6, 261 (2014).
36. Yushkevich, P. A. *et al.* Nearly automatic segmentation of hippocampal subfields in in vivo focal T2-weighted MRI. *Neuroimage* 53, 1208–1224 (2010).
37. Ding, S.-L., Song-Lin, D. & Van Hoesen, G. W. Organization and detailed parcellation of human hippocampal head and body regions based on a combined analysis of Cyto- and chemoarchitecture. *J. Comp. Neurol.* 523, 2233–2253 (2015).
38. Zeidman, P. & Maguire, E. A. Anterior hippocampus: the anatomy of perception, imagination and episodic memory. *Nat. Rev. Neurosci.* 17, 173–182 (2016).
39. Zhang, Y. and Brady, M. and Smith, S. Segmentation of brain MR images through a hidden Markov random field model and the expectation-maximization algorithm. *IEEE Trans Med Imag*, 20(1):45-57 (2001).
40. Yushkevich, P. A. *et al.* User-guided 3D active contour segmentation of anatomical structures: significantly improved efficiency and reliability. *Neuroimage* 31, 1116–1128 (2006).
41. Boccardi, M. *et al.* Delphi definition of the EADC-ADNI Harmonized Protocol for hippocampal segmentation on magnetic resonance. *Alzheimers. Dement.* 11, 126–138 (2015).

42. Frisoni, G. B. *et al.* The EADC-ADNI Harmonized Protocol for manual hippocampal segmentation on magnetic resonance: evidence of validity. *Alzheimers. Dement.* 11, 111–125 (2015).
43. Apostolova, L. G. *et al.* Relationship between hippocampal atrophy and neuropathology markers: A 7T MRI validation study of the EADC-ADNI Harmonized Hippocampal Segmentation Protocol. *Alzheimers. Dement.* 11, 139–150 (2015).
44. Jones, S. E., Buchbinder, B. R. & Itzhak, A. Three-dimensional mapping of cortical thickness using Laplace's Equation. *Hum. Brain Mapp.* 11, 12–32 (2000).
45. Sowell, E. R. *et al.* Longitudinal mapping of cortical thickness and brain growth in normal children. *J. Neurosci.* 24, 8223–8231 (2004).
46. Sapiro, G. *Geometric Partial Differential Equations and Image Analysis.* (Cambridge University Press, 2006).
47. Sethian, J. A. *Level Set Methods and Fast Marching Methods: Evolving Interfaces in Computational Geometry, Fluid Mechanics, Computer Vision, and Materials Science.* (Cambridge University Press, 1999).
48. Maass, A. *et al.* Functional subregions of the human entorhinal cortex. *Elife* 4, (2015).
49. Malykhin, N. V., Lebel, R. M., Coupland, N. J., Wilman, A. H. & Carter, R. In vivo quantification of hippocampal subfields using 4.7 T fast spin echo imaging. *Neuroimage* 49, 1224–1230 (2010).
50. Poppenk, J., Evensmoen, H. R., Moscovitch, M. & Nadel, L. Long-axis specialization of the human hippocampus. *Trends Cogn. Sci.* 17, 230–240 (2013).
51. Zeineh, M. M., Engel, S. A., Thompson, P. M. & Bookheimer, S. Y. Dynamics of the hippocampus during encoding and retrieval of face-name pairs. *Science* 299, 577–580 (2003).
52. Ekstrom, A. D. *et al.* Advances in high-resolution imaging and computational unfolding of the human hippocampus. *Neuroimage* 47, 42–49 (2009).
53. Suthana, N. A. *et al.* High-resolution 7T fMRI of Human Hippocampal Subfields during Associative Learning. *J. Cogn. Neurosci.* 27, 1194–1206 (2015).
54. Patenaude, B., Smith, S. M., Kennedy, D. N. & Jenkinson, M. A Bayesian model of shape and appearance for subcortical brain segmentation. *Neuroimage* 56, 907–922 (2011).
55. Fischl, B. *et al.* Whole brain segmentation: automated labeling of neuroanatomical structures in the human brain. *Neuron* 33, 341–355 (2002).
56. Goubran, M. *et al.* In vivo MRI signatures of hippocampal subfield pathology in intractable epilepsy. *Hum. Brain Mapp.* 37, 1103–1119 (2016).

57. Steve, T. A., Jirsch, J. D. & Gross, D. W. Quantification of subfield pathology in hippocampal sclerosis: a systematic review and meta-analysis. *Epilepsy Res.* 108, 1279–1285 (2014).
58. Maccotta, L., Moseley, E. D., Benzinger, T. L. & Hogan, R. E. Beyond the CA1 subfield: Local hippocampal shape changes in MRI-negative temporal lobe epilepsy. *Epilepsia* 56, 780–788 (2015).
59. Coras, R. *et al.* 7T MRI features in control human hippocampus and hippocampal sclerosis: an ex vivo study with histologic correlations. *Epilepsia* 55, 2003–2016 (2014).
60. Stensola, H. *et al.* The entorhinal grid map is discretized. *Nature* 492, 72–78 (2012).
61. Kjelstrup, K. B. *et al.* Finite scale of spatial representation in the hippocampus. *Science* 321, 140–143 (2008).
62. Nakamura, N. H., Flasbeck, V., Maingret, N., Kitsukawa, T. & Sauvage, M. M. Proximodistal segregation of nonspatial information in CA3: preferential recruitment of a proximal CA3-distal CA1 network in nonspatial recognition memory. *J. Neurosci.* 33, 11506–11514 (2013).
63. Lee, H., Wang, C., Deshmukh, S. S. & Knierim, J. J. Neural Population Evidence of Functional Heterogeneity along the CA3 Transverse Axis: Pattern Completion versus Pattern Separation. *Neuron* 87, 1093–1105 (2015).
64. Lu, L., Igarashi, K. M., Witter, M. P., Moser, E. I. & Moser, M.-B. Topography of Place Maps along the CA3-to-CA2 Axis of the Hippocampus. *Neuron* 87, 1078–1092 (2015).
65. Nakazawa, Y., Yuki, N., Alex, P., Tanaka, K. Z. & Wiltgen, B. J. Memory retrieval along the proximodistal axis of CA1. *Hippocampus* (2016). doi:10.1002/hipo.22596

## Appendix A: Manual and user-guided computational steps for hippocampal subfield labelling

### Criteria for automatic unfolding:

- Hippocampus should be split into 3 labels in the hippocampus: dark band, hippocampal grey matter, and cysts  
With 4 extra-hippocampal structure labels: border with the medial-temporal lobe cortex, medial edge of vertical component of the uncus, hippocampal-amygdalar transition area (HATA), and indusium griseum.
- Dark band should have no 'holes' in it when viewed in 3D (with no model smoothing).
- Dark band should be visible on the finished 3D model all along its medial edge and nowhere else.
- Hippocampal grey matter label should not contain or be touching any blank label except on its outer surface (i.e. no blank voxels inside hippocampus)
- Cyst label should only include CSF inside the hippocampus. If cysts are visible on the outside of the 3D model, they should be cleared.
- Extra-hippocampal structures should be labelled where they border the hippocampus (their entire structure can be labeled, but it's not necessary for segmenting hippocampal subfields).
- Consider how your manual segmentation is folded. If hippocampal grey matter from one fold contacts a different fold (e.g. in the digitations or along the curve of the uncus), then the automatic unfolding of the hippocampus will be incorrect (think of the Laplacian filter as 'leaking' through holes in the dark band or across overlapping folds).
- I HIGHLY RECOMMEND viewing the finished segmentation models I have provided (p025 and p073) in addition to the instructions here. Even better is to keep the model that most closely resembles a segmentation you are performing open in another window, as a reference.

### 1. Trace the hippocampal 'dark band'

The dark band separates the dentate gyrus on the inside from the outer subfields, and therefore the dark band should always be some distance inward from the hippocampal border, surrounded by hippocampal grey matter. The exception to this rule is along the medial side of the hippocampus, where the dark band terminates on the outer hippocampal border. The dark band may be obscured by hippocampal cysts, in which case it should be estimated and drawn in or the cyst label should

completely plug the hole. It's very easy to confuse dark band with alveus, particularly in the axial and sagittal planes. Thus, only dark areas which you are certain constitute dark band should be traced on the first pass, and fill in missing areas later. Where uncertain, make use of the other planes of view. I most often trace with a 2x2 paintbrush, but switch to 1x1 where the dark band appears only very thin or very faint. This label should be saved separately from the labels which will later be generated from it.

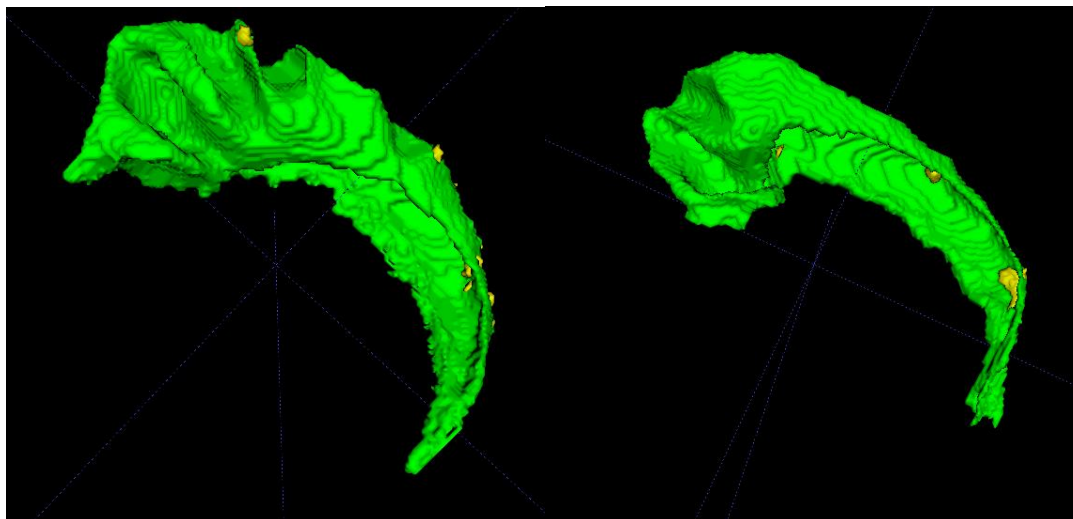


Fig 1.1. Models of a highly digitated hippocampus (left) and a less digitated hippocampus (right). Note that the yellow marks hippocampal cysts (see next step).

**Axial view.** In this view, at the approximate middle of the hippocampus, the hippocampus should look like a footprint, the anterior digitations being the toes. The dark band is just inward of the outer border, and should be traced only when it is clear, and only when it passes through the plane (as opposed to parts where it runs parallel to this plane, which will appear as larger, poorly defined dark blobs). I recommend starting in the middle of the hippocampus and working downward and then upward.

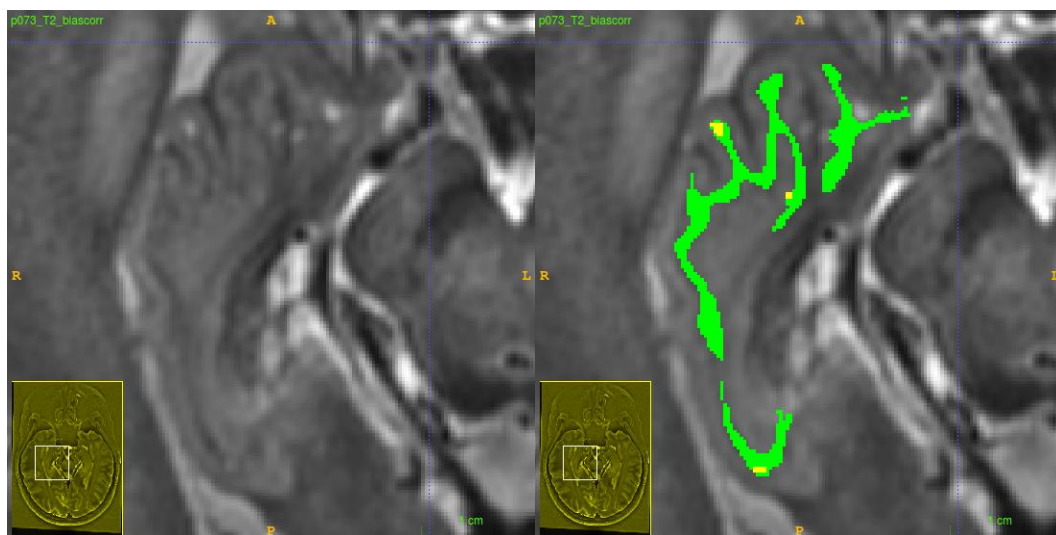
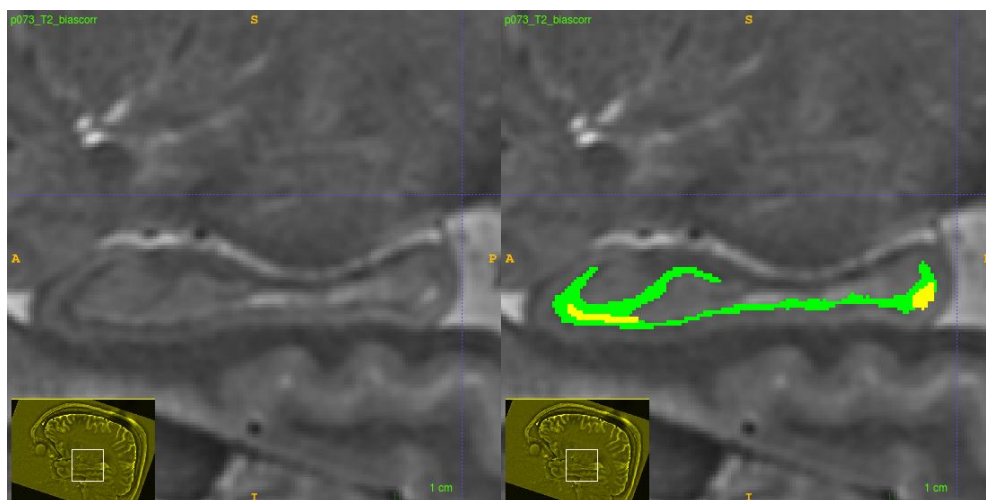


Fig 1.2. Axial view.

**Sagittal view.** The same rules as 1.2 apply here. There is no dark band over top of most of the subiculum in more medial views. This view should be used for tracing the hippocampal tail, which should be included as far posteriorly and medially as the dark band is obvious. Dilation of the dark band in the next step should include all the grey matter which touches the hippocampus, even if it appears to extend somewhat far posteriorly. You may need to relabel this far posterior grey matter as indusium griseum when labelling extra-hippocampal structures.



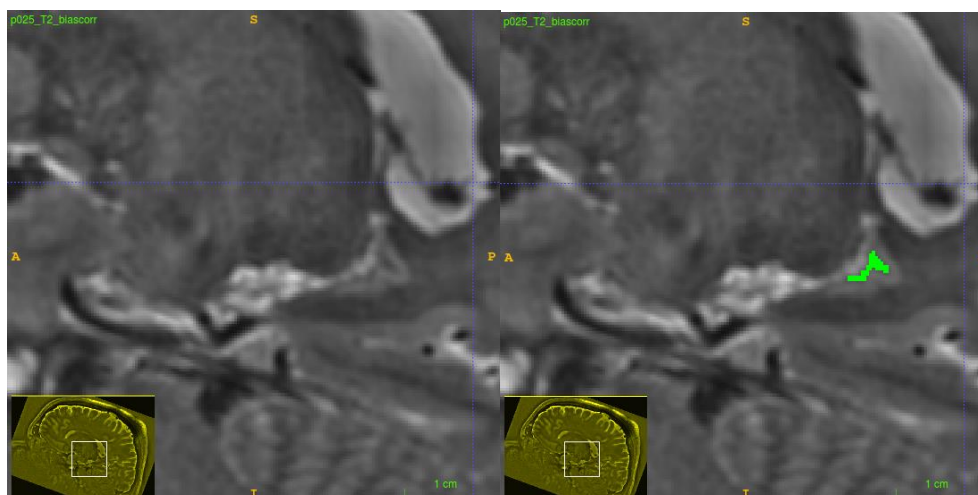


Fig 1.3. Sagittal view of dark band on the lateral side (top) and very medial side where only hippocampal tail is present (bottom)

**Coronal view.** This is where the dark band should be most clear in many cases, and should have a distinctive 'C' shape throughout the hippocampal body. In the head this shape is modified to extend into each digitation, and at the very most anterior the 'C' closes in on itself and becomes a single line. Note that at the superior side, the surface subfield CA3 often appears dark and so great care should be taken to separate dark band from CA3. In the uncus, the dark band may be very difficult to see, and so should be traced carefully.

After tracing what is visible in all slices, it should become clear from the model what parts of dark band were missed (remember that it is all one continuous tissue! Look for the holes). Try to fill in any large gaps, and when uncertain about how a piece of dark band connects to the rest of the dark band structure, see the other planes and the example segmentations I have provided. Note also that there should be an opening in the dark band along the medial side of the hippocampus along the entire anterior-posterior extent, up to roughly half-way through the hippocampal head where it closes. After the other subfields are traced, the dark band will still border the medial side of the hippocampus along the entire anterior-posterior extent except at the most anterior tip, around where the vertical component of the uncus (which will be traced in the next steps) is no longer visible. Looking through this opening, you should be able to see the concavity that the dark band forms enclosing the dentate gyrus.

Be sure to track tissues across different slices or across the different planes to determine what they are and that your labels line up correctly.

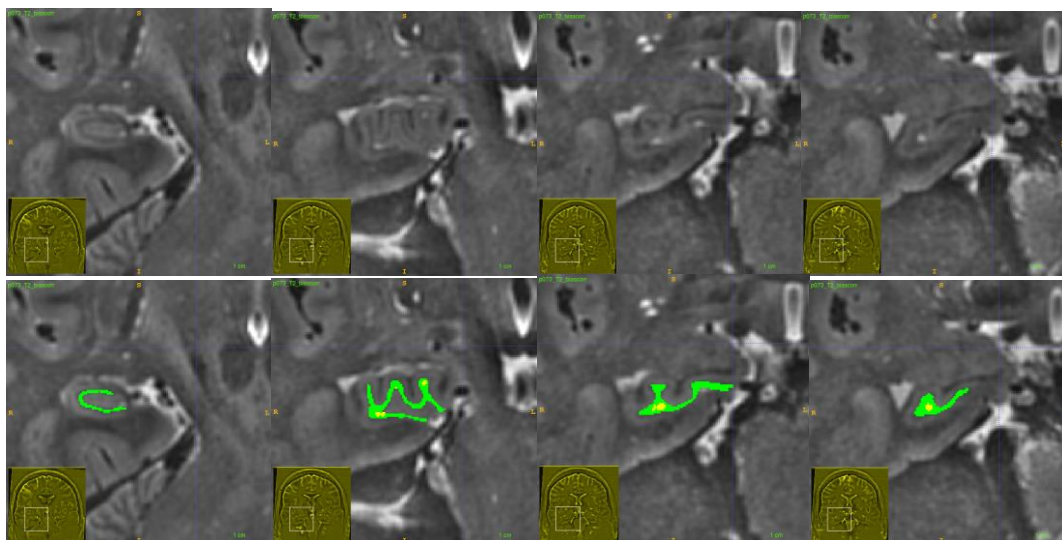


Fig 1.4. Coronal views of hippocampal dark band from posterior (left) to anterior (right).

**Touch-ups.** A good way to smooth dark band label and also fill in any small gaps is to dilate and then contract the entire label by a few voxels. This can be done using the ‘Snake’ tool in ITK-SNAP – use the edge attraction operation and set the filter options such that no edges are visible, then run a couple (~2-10) iterations of positive growth followed by iterations of negative growth. Make sure not to grow the label so much that different folds become connected!

Once you’re very confident in your tracing, you can try tracing only every other slice to save time. The dilation and contraction of the label will fill the gaps in between. Manual adjustments to the dark band can be made later too, so if uncertain then go to the next step.

Try to keep the dark band label thin! Contracting the label as far as possible without opening up gaps will be helpful to best capture only the dark voxels in the dark band.

## 2. Generate hippocampal grey matter label

The dark band label contains most of the spatial information we need – it enters into each digitation and runs parallel to the inferior, lateral, and much of the superior edge of the hippocampus (the medial and superior edges will still need some work).

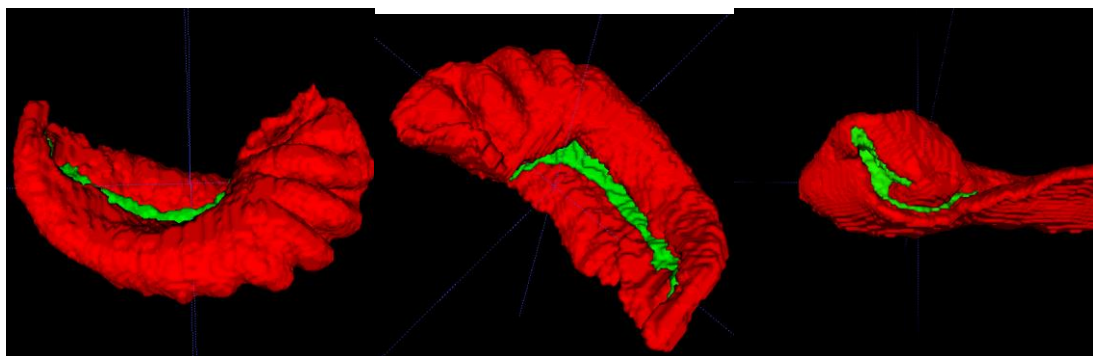
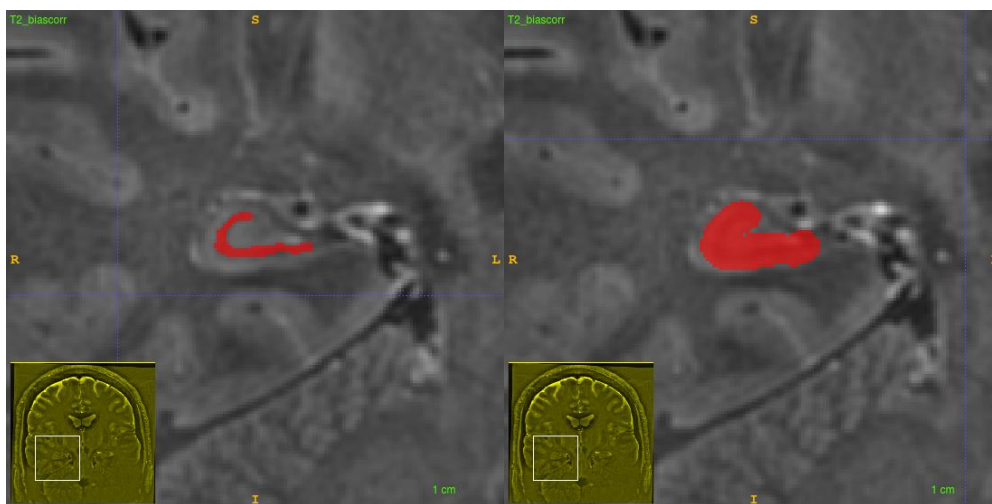


Fig 2.1. Whole hippocampus model, with the dark band visible in green along the medial side.

**Dilate the dark band.** This can be done in ITK-SNAP using the Snake tool. I've found the best way to do this is run unconstrained dilation to almost the outer edge of hippocampal grey matter, and then introduce some edge attraction constraints for the rest of the dilation. This avoids attraction to the dark band, but still allows grey matter thickness to vary slightly. The goal here is to best fit as many of the outer edges of the hippocampus as possible. Some edges, particularly the medial, will be wrong no matter what criteria you set so focus on the lateral, superior, and inferior borders.

Save this separately from the dark band label. Next combine your dark band label with this dilated label (for example, add the two label images together using FSL's `fslmaths` tool). The resulting label should contain 1's for whole hippocampus and 2's for dark band.



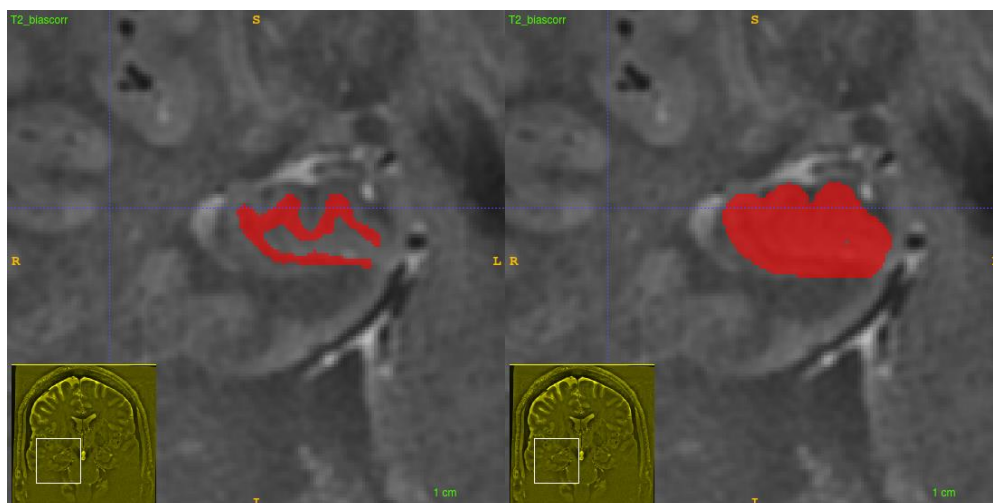


Fig 2.2. Dilation of dark band in the body (top) and head (bottom).

**Manual adjustments.** Along the superior edge, the dilation may have gone past the border of the hippocampus since the subfield present there – the CA3 – is typically thin. Thus it will have to be trimmed down, and may have to be extended slightly medially to fill in any additional grey matter that was missed. Similarly, dark blood vessels, alveus, and CSF are also often present medially to the dentate gyrus and superior to the subiculum and should be removed (see Fig. 2.3).

Some patches in the center of the hippocampus may have been missed, and some minor adjustments to the lateral and inferior borders are sometimes necessary. Additionally, the alveus entering in between each digitation is sometimes filled in because of too much dilation. This should also be manually removed such that label from one digitation is separated from other digitations by at least 1 voxel in all orientations (including diagonally). Dark band can also be manually adjusted while performing these adjustments.

Looking at the model, the dark band should be cleanly visible on the medial side. In the uncus, the dark band should still be visible and sometimes will run along the bottom of a the vertical component of the uncus such that a large area of dark band label is visible on the model. In these cases, make sure to remove all of the dilated hippocampal label inferior or medial to the dark band. The grey matter of the uncus should not contact the grey matter of the subiculum running below it - they should be separated by clear label or otherwise by dark band.

Because the hippocampal tail curves medially, the dark band will be visible on the anterior side.

The thresholding tool should be used across the entire hippocampus to relabel any cysts or CSF around the hippocampus as such. Be careful, grey matter intensities are

often high in the tail despite bias field correction. Look for round, light ‘patches’ that fade gradually into more typical grey matter and exclude the light parts. If this does not work well, simply label these cysts manually (I recommend a round, 4-voxel wide 3D brush). Where CSF is visible in one slice, there is also likely to be at least some partial voluming with CSF in the next slices.

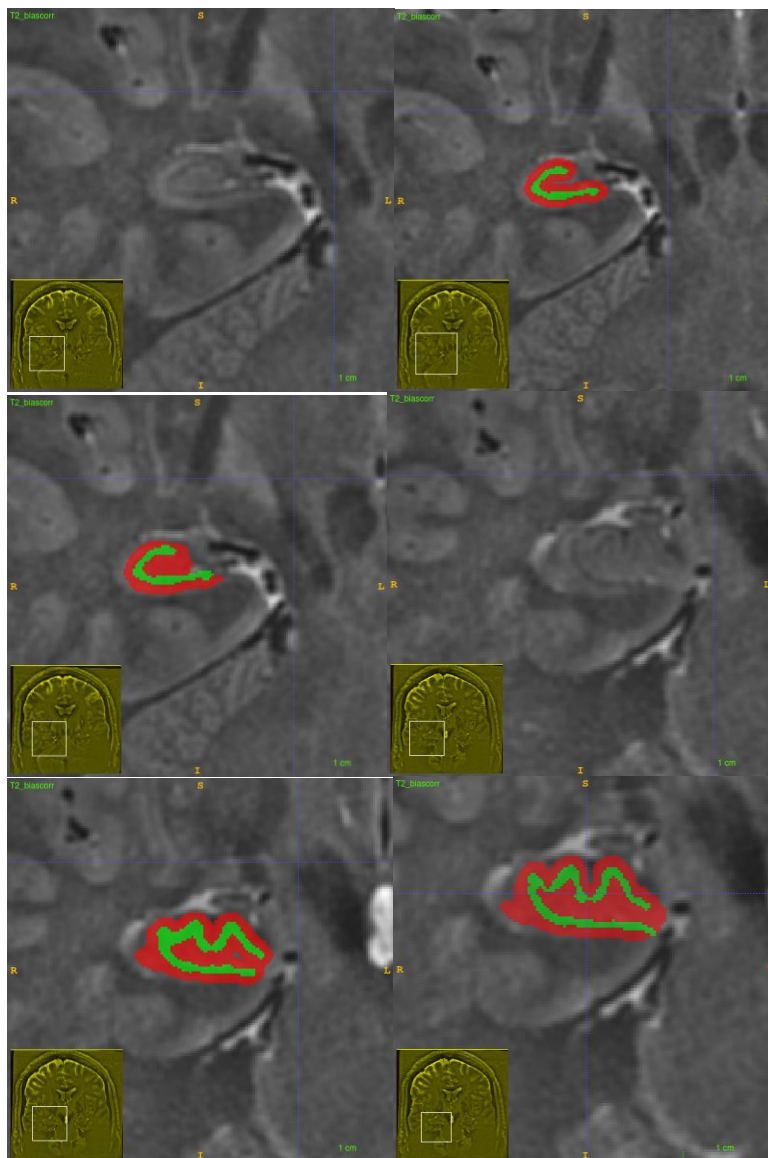


Fig 2.3. Examples of manual adjustments to be made to the whole hippocampus label in the body (top) and head (bottom).

**Subiculum.** The subiculum is typically dark, and is sometimes almost indistinguishable from white matter. However, even if it is difficult to distinguish, a band of tissue (~1mm in thickness) should extend medially from the hippocampus. It

runs below the CSF in the ventricle, and should not include partial voluming from the ventricle. Typically the most medial border of subiculum is the most medial extension of white matter, but where visible, this border can be adjusted to reach but not include the lighter grey matter tissue that makes up the entorhinal and parahippocampal cortices. In the hippocampal head, the subiculum runs almost entirely below the dark band and so not much will need to be added (though there should still be a small 'lip' visible extending downward and medially. This lip should be just below where the dark band is visible on the medial surface of the 3D model. In the hippocampal tail, the medial extension that is subiculum becomes shorter and shorter until it collides with the most medial, posterior edge of the tail.

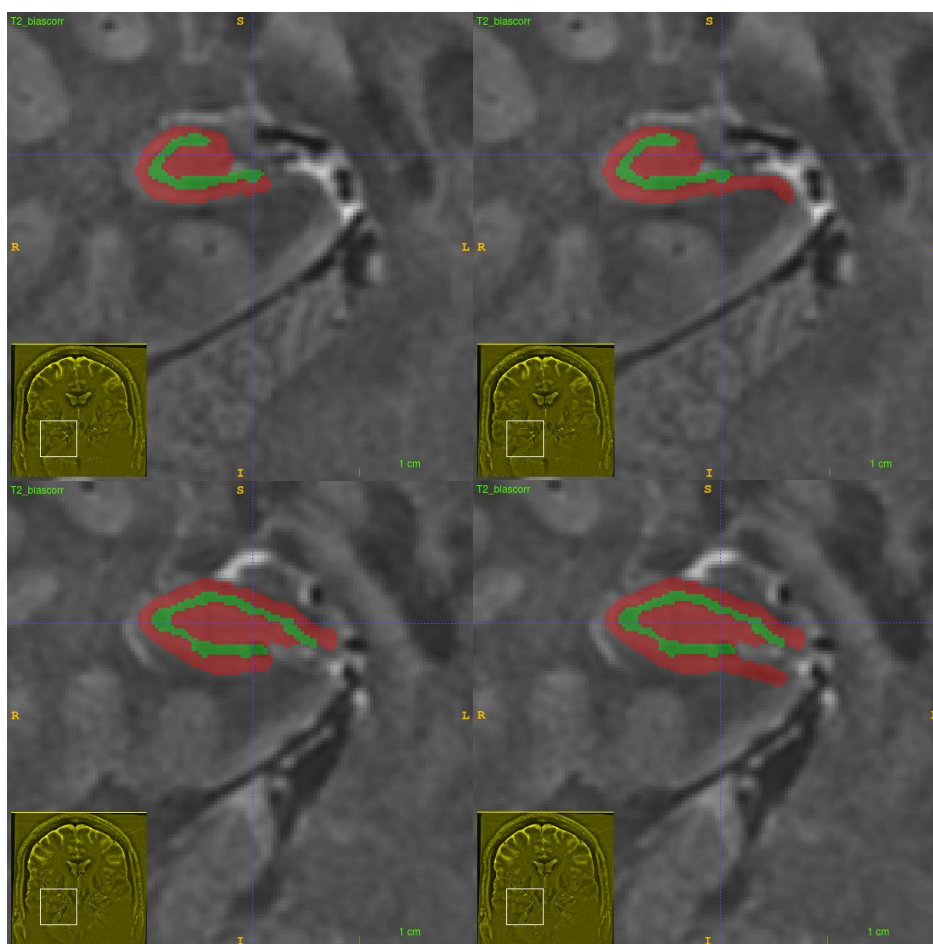


Fig 2.4. Image of medial extension making up the subiculum in the body (top) and head (bottom).

**Vertical component of the uncus.** This must be drawn in manually (or carefully grown in using the Snake tool). It is a thin layer of grey matter on the medial side of the uncus and separated from the rest of the uncus by white matter of the alveus. Often there is CSF medial to this, so be careful not to include partial volumed CSF. In

anterior slices the superior border is not clear, and should be drawn approximately halfway between the most superior part of the rest of the hippocampus and the lowest part of the amygdala. Past this is hippocampal-amygdala transition area. The vertical component of the uncus should become shorter in the most anterior until it is indistinguishable from the rest of the hippocampal head at roughly the same coronal slice as the dark band can no longer be seen on the medial side of the 3D model.

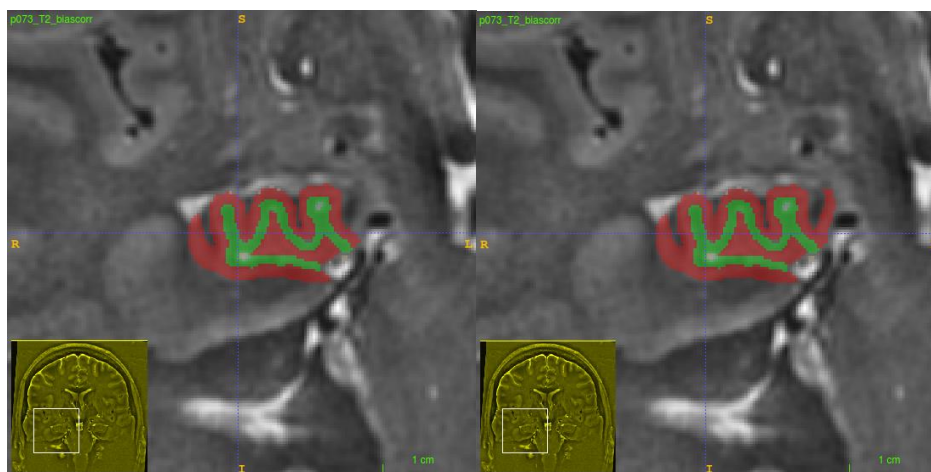
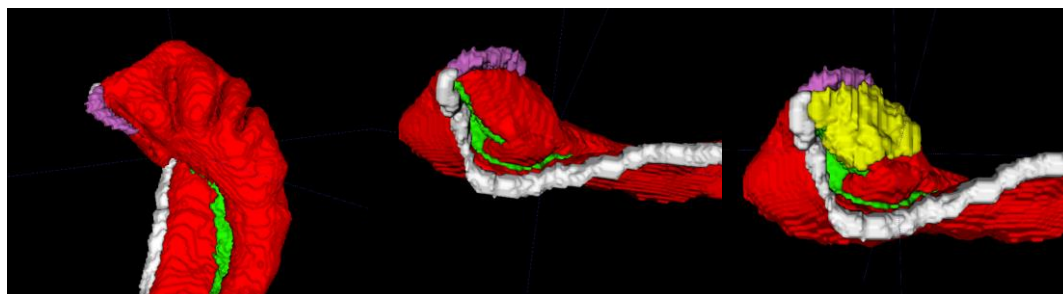


Fig. 2.5. Image of vertical component of the uncus.

### 3. Label extra-hippocampal structures

These aren't a part of the hippocampus, but are needed to mark the anterior, posterior, and medial edges of the hippocampus. Since these aren't the primary structures of interest here, I typically only label them only where they actually border the hippocampus. Each of these labels should contact the medial-temporal lobe cortex border label (so subsequent unfolding will be close to orthogonal).



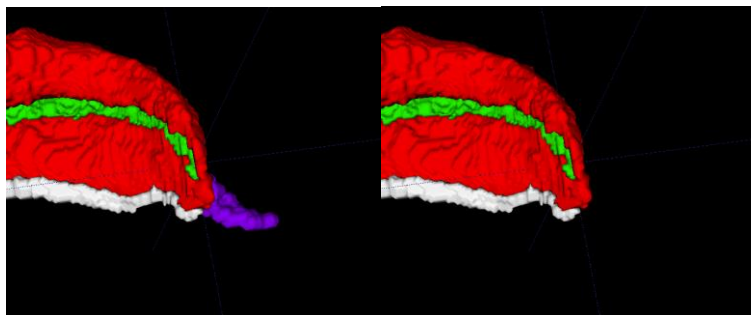


Fig 3.1. Extra-hippocampal structures in the head (top) and tail (bottom). The medial-temporal lobe cortex border is marked in white, HATA in pink, indusium griseum in purple, and the medial side of the vertical component of the uncus in dark green. Label includes only parts of their structure that border the hippocampus, except the indusium griseum - following this structure posteriorly makes it easier to find.

**Medial-temporal lobe cortex border.** This should border the medial edge of the subiculum. In the hippocampal head, it wraps upward and medially along with the subiculum, and terminates on the anterior terminus of the vertical component of the uncus (also where the hippocampal-amygdalar transition area ends). Note that the entorhinal cortex label should not touch the inferior side of the uncus (where it runs over the subiculum in the hippocampal head), except at the very anterior end of the entorhinal cortex label. At the posterior end, the border with parahippocampal cortex (same label as border with entorhinal cortex) should extend back until it hits the main 'C' shape of the hippocampus and contacts the indusium griseum label.

**Hippocampal-Amygdala Transition Area (HATA).** This should be marked on the grey matter on the superior edge of the vertical component of the uncus, just below and medial to the amygdala. Its posterior border is where the vertical component of the uncus is no longer connected to the amygdala, and its anterior border is where the vertical component of the uncus is no longer visible (also where the entorhinal cortex border terminates).

**Indusium griseum.** This is the grey matter that extends from the posterior and medial of the hippocampal tail. You may have already labeled part of this as hippocampal grey matter after dilating your dark band label. Relabel everything posterior to the medial curve of the hippocampal tail with this label.

**Medial edge of vertical component of the uncus.** The dark band actually extends upward along this tissue into the vertical component of the uncus, but cannot be seen because of partial voluming with CSF of the ventricles. Thus this label is defined

geometrically. It should completely cover hippocampal grey matter label where the vertical component appears as a single, thin layer of tissue. Make sure not to use a brush so large that it labels the lateral side of the vertical component of the uncus as well.

## Appendix B: Mathematical definitions of computational unfolding techniques

### 1. Laplacian equation

The Laplacian equation consists of a second-order partial differential equation for defining a scalar field  $\Psi$  with defined boundaries at S and S' (also called source and sink). In 3D Euclidean space, the equation is as follows:

$$\nabla^2 \Psi = \partial^2 \Psi / \partial x^2 + \partial^2 \Psi / \partial y^2 + \partial^2 \Psi / \partial z^2 = 0,$$

Where  $\Psi = \Psi_1$  on S and  $\Psi = \Psi_2$  on S'. Note that  $\nabla$  denotes a gradient and  $\partial$  denotes a differential. In our example, the scalar field  $\Psi$  will consist of hippocampal grey matter, S will consist of the border with the HATA, and S' will consist of the border with indusium griseum. We set  $\Psi_1$  as 0 and  $\Psi_2$  as 1000, so once the equation is solved all scalars in between will take on a value between 0 and 1000, such that a smooth, linear increase is seen between S and S'. In our case, we applied an averaging filter with many iterations on  $\Psi$ , with  $\Psi_1$  and  $\Psi_2$  remaining constant, until the field  $\Psi$  remained unchanging and the Laplace equation was true (we found 50 000 iterations was sufficient given our voxel size and the length of the hippocampus. Initializing this filtering with Fast Marching scalar field, described in the next section, can speed this process up by reducing the number of iterations required by a factor of 10). The averaging filter ignored values outside of hippocampal grey matter, effectively insulating the inner and outer surfaces of  $\Psi$  such that the filter must pass through each fold and digitation, rather than 'leaking' across them. The result is a smooth gradient that indexes hippocampal grey matter a while taking into account its folding and curvature.

### 2. Fast Marching algorithm

In principle, the Fast Marching method walks outward from a starting point or set of points, labelling the points it passes by with the time it would take to reach that point if travelling at a given speed from where it started. The Fast Marching algorithm is based

on the Eikonal Fire equation, which is also a second-order partial derivative and follows the equation:

$$|u(x)| = 1/f(x) \quad \text{for } x \in \Omega,$$

$$u(x) = 0 \quad \text{for } x \in \partial\Omega,$$

Where  $f(x)$  can be thought of as the speed of the marching, and  $u(x)$  can be thought of as the minimum amount of time required to reach a given point. Note that  $\epsilon$  denotes an element of the following set and  $\Omega$  denotes a set of points with some resistance at every point. The amount of resistance at each point determines the location of the shortest path, but the resistances within that path do not affect the length of the path (i.e. does not affect the time it would take to travel through that path at speed  $f(x)$ ). The fast marching algorithm solves this equation by starting at a known point in  $\Omega$  and marching outward along its path of least resistance while labelling points with the distance travelled. In our example, we set high resistance to be 1.00 outside hippocampal grey matter and 0.01 within hippocampal grey matter, so the Fast Marching was forced to follow the curvature and digitations in this tissue.

# Curriculum Vitae

## Jordan DeKraker

### Education

- Currently completing M.Sc in Behavioural and Cognitive Neuroscience at Western University
- B.Sc in Neuroscience Combined Honours at Carleton University
- French Immersion high school diploma (Parkside Collegiate Institute; studied since primary school)

### Academic Achievement

- Winner of five competitive research grants:
  - o Ontario Graduate Scholarship in 2015 (Western University)
  - o Canadian Graduate Scholarship – Master’s (NSERC) in 2014 (Western University)
  - o Undergraduate Student Research Awards (NSERC) in 2012 (Carleton University) and 2013 (Western University)
  - o Dean’s Summer Research Internship (Carleton University) in 2011
- Carleton Academic Scholarship for good high school grades and maintaining an overall GPA greater than A- (or 80%) in 2011 to 2014
- Queen Elizabeth II Aiming for the Top Tuition Scholarship from OSAP for outstanding high school academic achievement

### Research Achievement

- Master’s thesis (in progress) with Dr. Stefan Köhler of the Western University Psychology Department and Dr. Ali Khan of the Western University Biomedical Imaging Department
  - o Titled “Delineating subfields of the hippocampal head in 7-tesla structural MRI”. Study deals with the challenges of imaging and interpreting the complex structure of the human hippocampal head.
  - o Side project: piloting and optimizing of structural and functional MRI acquisition sequences which can be used in a 7-tesla MRI.
  - o Side project: Supervising of an undergraduate student, Sawayra Owais, in running a follow-up study to one of my previous projects. Also took part in training and data-analysis for this study.
- Honours thesis with Dr. Holahan
  - o Titled “The Processing of Sequential Memories and the Recruitment of Cortical Brain Regions in Remote Spatial Memory Recall”. Study elucidated the conditions under which memories which are initially hippocampally-dependent come to be supported by the cortex in rats.
- Help a summer research grant with Dr. Khler of the Western University Psychology Department (NSERC USRA grant in 2013)
  - o Worked on a psychophysiology project in humans studying the effects of encoding contexts on subsequent memory for words, and interactions with the peripheral nervous system. Work published (see Publication 1 below).
- Held two summer research grants with Dr. Holahan of the Carleton Neuroscience Department (Carleton DSRI grant in 2011, NSERC USRA grant in 2012)
  - o Did a variety of animal research on topics such as molecular changes in the hippocampus following Morris water maze pretraining, schizophrenia models and treatment using a dopamine aptamer, toxicology of phthalates, and effects of NMDA receptor antagonist MK801 on learning, mostly in rats. Work published (see Publications 2 and 3 below).

### Publications

- Fiacconi, C. M., Dekraker, J., & Köhler, S. (2015). Psychophysiological evidence for the role of emotion in adaptive memory. *Journal of Experimental Psychology: General*, 144(5), 925

- Davis-MacNevin, P. L., Dekraker, J., LaDouceur, L., & Holahan, M. R. (2013). Comparison of the MK-801-induced increase in non-rewarded appetitive responding with dopamine agonists and locomotor activity in rats. *Journal of Psychopharmacology*, 0269881113492029
- Mentioned in *Brian Research* for contributions to the study “Enhanced adolescent learning and hippocampal axonal projections following preadolescent spatial exposure to a water or dry maze” (Wartman *et al.*, 2012)

#### Talks

- “Unravelling Subfields of the Hippocampal Head with 7T MRI” at:
  - o Epilepsy Research rounds, Robarts Research Institute, 2016 (Western University)
  - o Coffee talk series, Brain and Mind Institute, 2016 (Western University)
- “Imaging the human hippocampal head with 7 Tesla MRI at ultra-high resolution” at:
  - o Epilepsy and Neuroscience Research Day, London, ON, Canada 2015 (Regional)

#### Poster Presentations

- “Unravelling Hippocampal Subfields with 7T MRI” at:
  - o London Imaging Discovery Day in London, 2015 (Regional)
- “Autonomic Contributions to Adaptive Memory” at:
  - o Cognitive Neuroscience Society in San Francisco, 2015 (International)
  - o Canadian Society for Brain, Behaviour and Cognitive Sciences in Ottawa, 2015 (National)
  - o Lake Ontario Visionary Establishment in Niagara Falls, 2015 (Regional)
  - o Inaugural Brain and Mind Symposium in London, 2015 (Western University)
- Honours thesis poster presentation at Poster Day in Ottawa, 2014 (Carleton University)

#### Leadership

- Vice President external and co-founder of the Carleton Neuroscience Society (CNS) 2012-2014
- Member of the Carleton University Varsity Fencing Team in the 2011, 2012, and 2013 seasons
- Winner of Athletic Bursary from Carleton in 2012/2013
- Member of the Society for Neuroscience Ottawa Chapter (2013-14); Cognitive Neuroscience Society (2015); and Canadian Society for Brain, Behaviour and Cognitive Sciences (2015)
- Volunteer for team RRRAvens United (2012) and A New RRRRA (2013) in the Rideau River Residence Association elections at Carleton University
- Tutor in Introductory Chemistry at Carleton University, 2011, 2012, and 2013